

Syracuse University

## SURFACE at Syracuse University

---

Theses - ALL

---

12-13-2022

# Data-driven Estimation of the Power Grid Inertia with Increased Levels of Renewable Generation Resources

Che Kai Chang  
*Syracuse University*

Follow this and additional works at: <https://surface.syr.edu/thesis>



Part of the [Electrical and Computer Engineering Commons](#)

---

### Recommended Citation

Chang, Che Kai, "Data-driven Estimation of the Power Grid Inertia with Increased Levels of Renewable Generation Resources" (2022). *Theses - ALL*. 656.

<https://surface.syr.edu/thesis/656>

This Thesis is brought to you for free and open access by SURFACE at Syracuse University. It has been accepted for inclusion in Theses - ALL by an authorized administrator of SURFACE at Syracuse University. For more information, please contact [surface@syr.edu](mailto:surface@syr.edu).

## ABSTRACT

The thesis investigates methods for estimating inertia in systems at different levels of renewable energy penetrations. Estimating renewable generators' inertia is challenging because their structures differ from traditional generators. Moreover, the power generated from renewable energy resources is not stable, depending on weather conditions. When a power grid has a disturbance, photovoltaic inverter control influences a power grid inertia by different controllers, such as power factor and reactive power control, to bring a power grid back to a steady state. The changing reactive power impacts the frequency, which strongly relates to inertia and increases the inertia estimation problem.

Several papers proposed different approaches to estimating renewable generators' inertia. The two main categories of estimating inertia are model-based and measurement-based methods. The model-based methods mimic an actual renewable generator behavior to calculate inertia. It is a complicated model specialized for specific renewable devices, but unlike the measurement-based methods, it can estimate the inertia in the steady state. The measurement-based methods find the patterns in measured data and use classification or regression functions to calculate inertia. A measurement model can monitor a power grid in real time. However, the method needs parameter oscillation, representing power imbalance in a power grid. This thesis proposes three measurement-based models to estimate inertia for systems under levels of photovoltaic systems: Symbolic Aggregate Approximation, Back Propagation Neural Network, and Minimum Volume Enclosing with a Gradient Descent Machine Model.

The measurement-based inertia estimation models need large-scale system measurement data. PowerWorld Simulator has a function to analyze the transient stability, which is utilized in this thesis to generate simulated data for this. Reducing photovoltaic output power can mimic the impact of weather changes. Different types of photovoltaic controllers have various

behavior.

The Symbolic Aggregate Approximation transfers continuous data into discrete data. The advantage of this method over other techniques is its ability to compress large-scale data and the reduced data storage requirements. Hence, the model demonstrates the best performance for estimating the inertia.

The Minimum Volume Enclosing Ellipsoid visualizes measurement data, including frequency, generator output power, and bus voltage, on a 3-dimensional space. The volume of the enclosed ellipsoid is the output that yields label inertia. During a fault in a power system, the volume of the ellipsoid increases. The Gradient Descent Model estimates an optimal regression curve to match volume with label inertia as the estimated inertia.

The Back Propagation Neural Network is a nonlinear classification method. With multiple layers and neurons, this method can efficiently cluster complex input features, such as the frequency of all buses and generator output power. The error between the estimated inertia and the label inertia is used to modify the branches' weight to reduce error. The disadvantage of the second and third models is that they do not have a better performance than the first one.

**Data-driven Estimation of the Power Grid Inertia with Increased  
Levels of Renewable Generation Resources**

by

Che Kai Chang

B.S, Chung Yuan Christian University, 2018

Thesis

Submitted in partial fulfillment of the requirements for the degree of Master of Science in  
Electrical Engineering

Syracuse University

December 2022

Copyright © Che-Kai Chang, 2022

All Rights Reserved

## ACKNOWLEDGEMENTS

Thanks to my advisor, Prof. Sara Eftekharnejad, I successfully completed my master's thesis. She instructed me carefully from the beginning to the end of my research. Her conscientious attitude profoundly influences my research. Without her constant encouragement and support, I could not have overcome many difficulties.

Meanwhile, I would like to thank my family members. My parents, Chih Yung Chang and Shu Chen Yang, provide whole love and care to support me in studying at Syracuse University. My brother's family, Chen Hao Chang and Ting Ting Yang, assisted me in completing my academic research.

Also, I would like to thank Prof. Victor H Duenas, Prof. Jay Kyoon Lee, and Prof. Reza Zafarani for being members of my committee members. I was able to improve my thesis from their professional advice and support.

Finally, I thank my Smart Grid Research Lab friends, Dr. Rui Ma, Cheng Lyu, Nathalie Uwamahoro, and Ahmed Abyadh. Because of their encouragement and support, I could get some inspiration to put in my research and keep doing my research. Thank you for giving me a good memory at Syracuse University.

# TABLE OF CONTENTS

<b>Abstract</b>	<b>1</b>
<b>Acknowledgements</b>	<b>v</b>
<b>List of Figures</b>	<b>viii</b>
<b>List of Tables</b>	<b>x</b>
<b>1 Introduction</b>	<b>1</b>
1.1 Literature Review . . . . .	1
1.1.1 Virtual Inertia . . . . .	2
1.1.2 Estimation of the Virtual Inertia . . . . .	2
1.2 Thesis Outline . . . . .	6
1.3 Background . . . . .	7
1.3.1 Power Grid Stability . . . . .	7
1.3.2 Reliability Requirement . . . . .	8
1.3.3 Swing Equation . . . . .	8
1.3.4 Virtual Inertia . . . . .	10
1.4 Types of Controllers . . . . .	11
1.4.1 Power Factor Control . . . . .	11
1.4.2 Calculation of the power factor . . . . .	11
1.4.3 Reactive Power Control . . . . .	14
1.4.4 Voltage Control . . . . .	15
<b>2 Models Used for Simulation</b>	<b>17</b>
2.1 Synchronous Generator Model . . . . .	17
2.1.1 Machine Model . . . . .	17
2.1.2 Exciter Model . . . . .	18
2.1.3 Governor Model . . . . .	19
2.2 Model of the Renewable Generator . . . . .	19
2.2.1 Wind Generators Model . . . . .	21
2.2.2 Photovoltaic Model . . . . .	21

2.3	PowerWorld Simulation . . . . .	25
2.3.1	The Primary Control Stage . . . . .	26
2.3.2	PV Regulation . . . . .	28
2.4	PMU Measurement Data . . . . .	29
<b>3</b>	<b>Inertia Estimation</b>	<b>31</b>
3.1	Symbolic Aggregate Approximation . . . . .	31
3.1.1	K-nearest Neighbors Algorithm . . . . .	33
3.1.2	Inertia estimation . . . . .	34
3.2	Other Methods . . . . .	35
3.2.1	Back Propagation Neural Network . . . . .	35
3.2.2	Minimum Volume Enclosing Ellipsoid with a Gradient Descent Machine Learning Model . . . . .	40
<b>4</b>	<b>Sensitivity Analysis</b>	<b>44</b>
4.1	Scenario 1: Distributed PV Penetration of 3% . . . . .	44
4.2	Scenario 2: Distributed PV penetration of 10% . . . . .	46
4.3	Scenario 3: Large-scale PV penetration of 10% . . . . .	47
4.4	Scenario 4: Large-scale PV penetration of 40% . . . . .	49
4.5	Scenario 5: Large-scale PV penetration of 50% . . . . .	50
<b>5</b>	<b>Summary and Future Work</b>	<b>52</b>
5.1	Contributions . . . . .	52
5.1.1	Summary . . . . .	53
5.2	Future Research Directions . . . . .	54

**References**



## LIST OF FIGURES

1.1	Power factor control . . . . .	12
1.2	A two-bus power grid . . . . .	13
1.3	Two buses power grid . . . . .	15
2.1	Machine Model [56] . . . . .	18
2.2	IEEET1 exciter model [57] . . . . .	19
2.3	TGOV1 Governor Model [58] . . . . .	20
2.4	PV Machine Model [59] . . . . .	22
2.5	Power factor control [59] . . . . .	24
2.6	Reactive power controller [59] . . . . .	24
2.7	Voltage controller [59] . . . . .	24
2.8	IEEE 37-buses power grid . . . . .	25
2.9	The moment when a disturbance happens. . . . .	26
2.10	Frequency curves without inverter control . . . . .	29
2.11	Frequency curves with inverter control . . . . .	29
3.1	Illustration of SAX . . . . .	32
3.2	Illustration of dividing PMU measurement into time windows . . . . .	32
3.3	K-nearest Neighbor algorithm model . . . . .	33
3.4	RMS error for regression and classification functions with different $K$ values	34
3.5	Illustration of a Back Propagation Neural Network . . . . .	35
3.6	Illustration of the loss function and learning rate (Y: Loss function, X: weight values) . . . . .	36
3.7	With a same initial weight of branches . . . . .	36
3.8	With a random initial weight of branches . . . . .	37
3.9	Illustration of the Sigmoid function . . . . .	38
3.10	Illustration of a simple network . . . . .	38
3.11	Illustration of the impact of the number of neurons in RMS error . . . . .	40
3.12	Illustration of finding a Minimum Volume Ellipsoid . . . . .	41
3.13	The error between the regression function and label inertia . . . . .	43

4.1	Illustration of estimated errors of the inertia estimation methods in the first scenario . . . . .	45
4.2	Illustration of errors of SAX in the first scenario . . . . .	45
4.3	Illustration of estimated errors of inertia estimation methods in the second scenario . . . . .	46
4.4	Illustration of errors of SAX in the second scenario . . . . .	47
4.5	Illustration of estimated errors of inertia estimation methods in the third scenario	48
4.6	Illustration of errors of SAX in the third scenario . . . . .	48
4.7	Illustration of estimated errors of inertia estimation methods in the fourth scenario . . . . .	49
4.8	Illustration of errors of SAX in the fourth scenario . . . . .	49
4.9	Illustration of estimated errors of inertia estimation methods in the fifth scenario	50
4.10	Illustration of errors of SAX in the fifth scenario . . . . .	51

## LIST OF TABLES

2.1	Lowest frequency points(replace one synchronous generator) . . . . .	27
2.2	Lowest frequency points(replace two synchronous generators) . . . . .	28
2.3	Lowest frequency points(replace three synchronous generators) . . . . .	28
3.1	RMS error for different structures . . . . .	43
4.1	RMSE for inertia estimation methods . . . . .	46
4.2	RMSE for different inertia estimation approaches . . . . .	47
4.3	RMSE for different inertia estimation approaches . . . . .	48
4.4	RMSE for different inertia estimation approaches . . . . .	50
4.5	RMSE for different inertia estimation approaches . . . . .	51

# Chapter 1

## Introduction

### 1.1 Literature Review

Clean energy from renewable energy resources, such as solar and wind, results in reduced greenhouse gas emissions. However, due to their intermittency, these resources cannot continuously supply power to the grids. An imbalance of power between generation and loads will lead to grid instability. Therefore, when renewable energy resources are used as the main sources of generation, they cannot ensure grid stability at all times.

Traditional synchronous generators are equipped with turbines to store and release kinetic energy to compensate for power imbalance throughout the system. Load and solar energy can be regarded as the demand side of a power system, and they cause electrical power deviation. Meanwhile, synchronous generators cannot suddenly change turbines' parameters to generate additional energy. Therefore, turbines release kinetic energy to compensate for the electrical power deviation, causing a drop in frequency. Although some photovoltaic (PV) generation systems are equipped with energy storage devices to compensate for power imbalance, these devices are expensive and require large capital investments by utilities. Therefore, it is essential to adjust power generation from other resources in systems with high levels of PV generation. Depending on the level of power generated by the PV systems, specific requirements for the PV systems are defined. Most distributed photovoltaics are equipped with batteries to avoid stability problems, and large-scale photovoltaics must respond to power grids to prevent system collapse [1].

### 1.1.1 Virtual Inertia

Unlike synchronous generators, PV systems do not have a rotating mass. Therefore, the Swing Equation cannot be applied to calculate the inertia of PV systems. In a steady state, PV generators do not need to compensate for the grid. Hence, these devices do not contribute to the system inertia. During disturbances, the inverters are capable of providing reactive power support and, as a result, contribute to the change of output frequency and moment of inertia. The moment of inertia is referred to as the virtual inertia due to similar behavior as the conventional turbine [2].

### 1.1.2 Estimation of the Virtual Inertia

A general method to estimate the virtual inertia is to calculate the relationship between frequency variation and power deviation. For example, a PV system with low virtual inertia cannot recover the frequency after a disturbance occurs because it does not contain enough kinetic energy for regulation purposes. Using the frequency change ( $\frac{df}{dt}$  per unit) and power deviation ( $\Delta P$ ), equation (1.1) can approximately estimate the virtual inertia ( $H$ ). The majority of the available literature in this domain use the general method as labels for training other methods [1].

$$\Delta P = \frac{2H}{f_0} \frac{df}{dt} \tag{1.1}$$

However, inverter controllers use frequency and the generated power as inputs, voltage, and power factor, among other parameters, to control the output power. As a result, the conventional methods of inertia estimation can only approximately estimate the virtual inertia due to only considering the frequency and the generated power in calculations [3].

Considering multiple input features, two types of inertial estimation methods can estimate virtual inertia: model-based and measurement-based [4]. The model-based methods establish models to simulate the dynamic models of PVs [5]. Unlike measurement-based methods, model-based methods can accurately estimate virtual inertia without using phasor measurement units (PMUs) to provide system measurements. However, model-based methods are complex and specific to certain types of inverter-based resources (IBRs), and, therefore, cannot be applied to different types of devices. The measurement-based methods use PMU data to estimate the virtual inertia. Most measurement-based methods use machine learning models to cluster or regress PMU data, to estimate the virtual inertia in near real-time. However, these methods cannot estimate inertia in steady-state because they require a change in input features to generate results [4].

## Model-Based Inertia Estimation

Various model-based methods have been proposed in the literature. The model-based methods that are based on the Kalman filter methodology predict the parameters of the generator or the control unit [5, 6, 7, 8]. In [9] and [10] the Kalman filter is replaced with a nonlinear least square method to estimate the generator parameters. Other works, such as those presented in [11, 12, 13], proposed various Kalman Filter methods to update measurement function to predict system parameters. Other works have extended this approach of estimating inertia to multiple synchronous generators [14, 15, 16].

Algebraic differential equations are another common model-based approach for estimating inertia [17]. For multiple generators, coherency-based methods and area detection are proposed for estimating inertia by grouping generators with a similar dynamic performance in a power grid. The generators in each group exhibit similar behavior on output parameters,

such as frequency. Different equations, representing different dynamic models can then be used to estimate the system inertia. In [18], the Discrete Fourier transform is used to analyze the frequency curve to build equations for different dynamic models. In other works [19, 20], equivalent dynamic models are developed to represent multiple areas and estimate inertia. When a disturbance occurs, generators regulate the power grid to stabilize the grid. The process includes the primary and secondary control stages, each with a different regulation strategy. Based on this behavior, the authors in [21] analyze the behavior of generators in each stage and propose to use different equations to estimate inertia.

Most model-based models can estimate inertia without significant disturbances, but they have some weaknesses. Most generators have multiple parameter controllers, increasing dynamic models' complexity. Therefore, the linear system state function is unsuitable for predicting system parameters. Using a non-linear system state function will need a proper method for prediction, such as the Extended Kalman Filter method and the Unscented Kalman Filter method. Those complicated models update their measurement functions and cannot estimate the virtual inertia in a few iterations.

## **Measurement-Based Inertia Estimation**

The authors in [22] presented a strategy to estimate inertia based on real-time data to calculate the inertia of photovoltaic systems. The method utilizes a Multivariate Random Forest Regressor to evaluate system inertia. The load profile, frequency feature, weather data, and inertia data are the inputs used to train the machine learning model. Similarly, in [23], an online method is proposed to estimate inertia from PMU measurements. The method uses a system identification model to find the system state and calculate the inertia. In addition, the work presented in [24] used a system identification model to estimate inertia. First, the identification model, the state space model, finds the change of parameters in a power grid, such as electrical power deviation and the rate of change of frequency. Then, convert

the identification model into a transfer function to calculate inertia. A Minimum Volume Enclosing Ellipsoid model is used to extract features from the PMU data. First, time series data is divided into several time windows, and bus frequency data is collected for each time window. Next, the N-bus frequency data are transformed into an N-dimension space. The volume of the enclosing ellipsoid is estimated, which acts as the input feature of a machine learning model. The advantage of this model is its ability to compress large-scale data. A similar concept is deployed in [25] to estimate inertia from phasor measurement units. Unlike other papers, the method presented in [25] uses a decision tree to classify dynamic events. The authors in [26], used transfer functions from PMU measurement to calculate the inertia on non-synchronous devices. In another research, the Kalman filtering approach is used to estimate system inertia from PMU data [27]. In another approach the works presented in [28, 29] use a higher-order polynomial approximation to model the change of frequency and eventually estimate inertia.

Dynamic system parameters can also be deployed for estimating system inertia. for example, in [30, 31, 32, 33], the least squares method is used to estimate various dynamic parameters, including system inertia, from wide-area measurement data. The authors in [34] developed an inertia estimation method based on linearized dynamic equations that are derived from eigenstructure analysis in multiple areas of the power system. Similarly, the works presented in [35] and [36] build dynamic equations to estimate inertia from ambient measurement data. First, a power grid is divided into several areas with similar dynamic devices. Then, system identification techniques are used to identify models from a database. Finally, the resulting transfer function is deployed to estimate system inertia. Similar works can be found on system identification methods as a tool for estimating system inertia [36, 37, 38, 39] from system measurements.

In a different approach, the methods presented in [40] and [41] estimate inertia from genera-



tors' parameters, including active power and derivative of frequency. These methods extract information from two time windows to calculate the deviation in system parameters and estimate the equivalent inertia. This approach can be extended to multiple generators and is robust to the changes in the width of the time windows. The authors in [42] proposed a similar method to estimate inertia in an energy storage system based on a moving horizon approach.

Measurement-based models are convenient because the input is PMU measurement. Most models use system identification models to find transfer functions between parameters, such as frequency and electrical power deviation. Then, calculate the inertia from transfer functions. However, models are influenced by noise and numerical problems. Some methods use filter models to filter out the noise and provide limitations to avoid numerical problems.

## 1.2 Thesis Outline

The thesis proposes a new method to estimate inertia based on a measurement-based model. Unlike other measurement-based models, the method has a better estimating result in reducing the influence of numerical problems. The thesis is structured as follows: Chapter 1 shows the background of power grid stability and different control types, Chapter 2 shows the synchronous generator and photovoltaic models used in simulations, Chapter 3 compares and develops three inertial estimation methods, and Chapter 4 shows the sensitivity of these estimation methods to various system parameters. Chapter 5 provide the summary, contributions, and future work.

## 1.3 Background

### 1.3.1 Power Grid Stability

Integration of increased levels of photovoltaic generation to a power grid is expected to adversely affect the stability of the grid due to the intermittency of the output power from PV systems and the lack of system inertia [43, 44]. The imbalance between the generated power and the consumed power will affect the power grid stability, and the synchronous generators will compensate for the power imbalance between the loads and the total generation. A low-inertia power grid cannot withstand a significant power imbalance due to low kinetic energy storage. If proper control strategies, such as inverter-based controls, are not in place, load shedding could be the last resort in preventing blackouts. The decline in stability is explained by the fact that the PV systems have no rotating unit and cannot release or store kinetic energy to compensate for a power imbalance. At the same time, the recovery capacity of the synchronous generators is reduced as a portion of the generation portfolio of these resources is replaced by inverter-based resources. With the replacement of more synchronous generators, the stability problem becomes more severe.

The power electronic-based inverters can control the output power of PV systems to prevent a power grid from collapsing and adjust parameters such as frequency, voltage, and reactive power after a disturbance occurs. For example, when renewable generators reduce the output power due to weather changes, synchronous generators must provide additional power to compensate for the load. However, turbines cannot quickly respond to the power imbalance and slow down the rotational speed to generate more output power. Therefore, the power grid frequency drops and needs to be regulated back to the nominal value. Synchronous generators have governor controllers to enhance more steam to push turbines to increase the rotational speed [45]. Meanwhile, PV inverters utilize switches signals to increase the frequency of output AC power [46].

### 1.3.2 Reliability Requirement

The Federal Energy Regulatory Commission (FERC) and the North American Power Reliability Corporation (NERC) have established standards to ensure power grid reliability. To maintain the power factor, FERC proposed the standard (Order 661A) for renewable generators to maintain the power factor, including wind farms and PV, which produce over 20 megawatts. The power factor comes from equation (1.2), and the value should be between 0.95 and 1.05 [47].

$$\text{power factor} = \frac{\text{Real power}}{\text{Rated power}} \tag{1.2}$$

A wind farm must provide sufficient dynamic voltage to maintain the stability of the grid. Although this requirement does not apply to photovoltaic systems, most customers follow this requirement. NERC also requires that renewable generators provide more than 20 MW of control voltage and reactive power [48]. Moreover, according to the Institute of Electrical and Electronics Engineers (IEEE 1547 standard), a PV system larger than 10 MW should respond to power deviations within the system [47].

### 1.3.3 Swing Equation

The Swing Equation, shown in equation (1.1), is the equation of motion for synchronous generators. The moment of inertia comes from the turbine acceleration and two torques, i.e., the mechanical and electrical torques. In steady-state, the mechanical torque matches the electrical torque. Therefore, all parameters are constant. However, in equation (1.3), when the weather condition changes, PVs reduce the output power and cause synchronous generators

to generate additional electrical energy( $\Delta P_{synchronous}$ ) to balance the load demand( $\Delta P_{load}$ ). As mentioned, turbines cannot suddenly change the output power and inertia constant( $M$ ), so turbines change the rotational frequency( $\omega$ ) to compensate for the power imbalance [49].

$$\Delta P_{synchronous} = \frac{1}{2}M\omega^2 + \Delta P_{load} \quad (1.3)$$

Furthermore, the output power and frequency can express from the turbine side in equation (1.4). Input resources, such as steam, push turbines to generate mechanical power( $P_m$ ). Turbines rotate their blades and generate electrical power( $P_e$ ) due to electromagnetic induction. If the rotational velocity increases( $\frac{d^2\theta_m}{dt^2}$ ), the generator injects more power into a grid.

$$J\frac{d^2\theta_m}{dt^2} = P_a = P_m - P_e \quad (1.4)$$

The parameter  $\theta$  in the swing equation represents the phase angle between the rotor and the stator,  $P_a$  represents the accelerating power, which is the difference between the mechanical and electrical power, and  $J(sec)$  represents the moment of inertia. Moreover, in equation (1.5), the inertia constant( $H$ ) represents the ratio of released energy to the base power( $S_B$ ), which is the maximum output power. The released energy comes from rotational energy( $E_{kinetic}$ ) from turbines, including frequency( $f$ ) and the moment of inertia( $J$ ).

$$H = \frac{E_{kinetic}}{S_B} = \frac{J(2\pi f)^2}{2S_B} = \frac{J\omega^2}{2S_B} = \frac{J\frac{d^2\theta}{dt^2}}{2S_B} \quad (1.5)$$

Generally, there are several generators( $S_{B,i}$ ) in a power grid. Hence, the equivalent inertia that represent the inertia of the entire grid can be shown as equation (1.6) [50].

$$H_{eq} = \frac{\sum H_i S_{B,i}}{S_B} \quad (1.6)$$

### 1.3.4 Virtual Inertia

While the PV systems do not contribute to system inertia in the same way as traditional synchronous generators, the power electronic inverters can mimic the inertial response during transient stability. hence, the inverter-based resources can contribute to what is referred to as virtual inertia. The Swing Equation cannot be applied to nonrotating equipment. Therefore, there is a need for methods that can estimate the virtual inertia supplied by the inverter-based resources. Moreover, a steady-state power grid does not have virtual inertia because the photovoltaic inverter controllers are inactive without disturbances. When a disturbance occurs, the frequency oscillates, and PV inverters compensate for the frequency change. As shown in equation (1.7), the virtual inertia can be approximated with the rate of change of frequency and the deviation of the electric power [50]. However, other parameters are not included. This thesis develops a new data-driven approach to estimating virtual inertia. Historical inertia data will be used as labels while various machine learning models are trained with frequency variations and deviation of the electric power as inputs. Inverters can control terminal voltage, power factor, or reactive power. Hence, to further improve the accuracy of inertia estimation, these parameters can also be included in training the models. In this thesis, Symbolic Aggregation Approximation (SAX) [51], Minimum Volume Enclosing Ellipsoid(MVEE) [24], and back-propagation neural networks [52] are used that use multiple input features to train models and estimate virtual inertia.

The label inertia comes from equation (1.7) to train three methods. The transfer function determines the inertia from frequency and power changes. The mechanical power( $\Delta P_m$ ) does not change during a short time, so  $\Delta P_m$  is zero.  $\Delta P_e$  and  $\Delta f$  come from PMU

measurement [50].

$$\frac{d\Delta f}{dt} = \frac{1}{2H}(\Delta P_m - \Delta P_e) \quad (1.7)$$

## 1.4 Types of Controllers

Different types of controllers exist to regulate the power grids after a disturbance occurs. In large-scale photovoltaic systems, three controllers exist to regulate the power factor, reactive power, and voltage.

### 1.4.1 Power Factor Control

The power factor in figure (1.1), i.e.,  $Power\ factor = \frac{Real\ power}{Apperent\ power}$ , represents the relation between the real power and the reactive power. Although some load demands require real power, inductive loads, such as transmission lines, consume reactive power. Furthermore, reactive power can help regulate voltage in transmission lines and reduce the voltage collapse risk.

In systems with high levels of photovoltaic power generation that mainly generate real power, there are significant power factor problems due to the fact that fewer synchronous generators are available to generate reactive power. In other words, if PV systems do not provide enough reactive power, synchronous generators must produce more reactive power to meet demand. Therefore, PV systems must contribute to the total reactive power of the system to prevent stability issues within the system [53].

### 1.4.2 Calculation of the power factor

In figure (1.2), a transmission line, modeled as a series impedance  $|Z|\angle\gamma$ , connects a generator and a power grid. The generator determines the real and reactive power delivered to the power

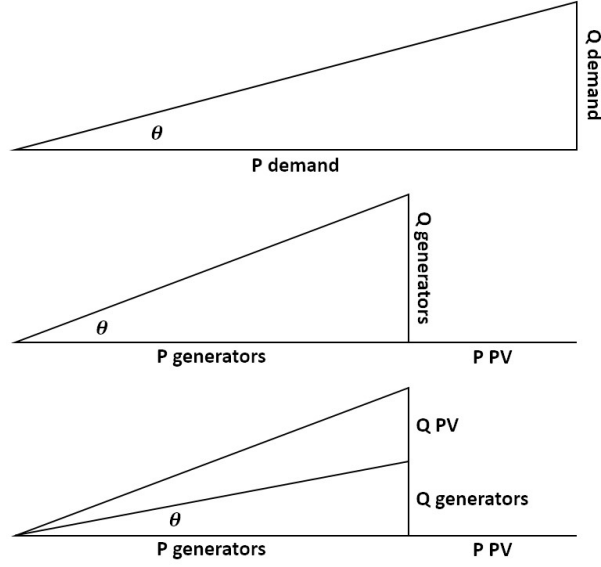


Figure 1.1: Power factor control

grid to maintain the zero power angle on the second bus. The injected three-phase power ( $S_{3\phi}$ ) is equally divided between the three phases, and the single-phase current ( $I_{singlephase}$ ) is calculated according to equation (1.8).

$$I_{single\ phase} = \frac{|E|\angle\delta - |V|\angle 0}{|Z|\angle\gamma} \quad (1.8)$$

The injected power on the power grid is equal to the product of voltage ( $V\angle 0$ ) and conjugate of current ( $I_{singlephase}^*$ ), as shown in equation (1.9). Hence, the real and reactive powers can be calculated according to equations (1.10) and (1.11).

$$S_{3\phi} = 3VI_{single\ phase}^* = 3\frac{|E||V|\angle\gamma - \delta}{|Z|} - 3\frac{|V|^2\angle\gamma}{|Z|} \quad (1.9)$$

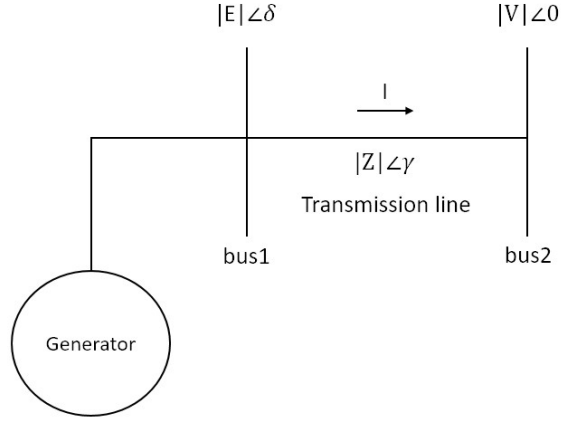


Figure 1.2: A two-bus power grid

$$P_{3\phi} = 3 \frac{|E||V|}{|Z|} \cos(\gamma - \delta) - 3 \frac{|V|^2}{|Z|} \cos(\gamma) \quad (1.10)$$

$$Q_{3\phi} = 3 \frac{|E||V|}{|Z|} \sin(\gamma - \delta) - 3 \frac{|V|^2}{|Z|} \sin(\gamma) \quad (1.11)$$

The reactance is negligible ( $\gamma = 0$ ) if the transmission line does not have a large reactance. Under these circumstances, the power equations are simplified to result in equations (1.12) and (1.13). The angle of power on bus 1 is therefore calculated from equation (1.14).

$$P_{3\phi} = 3 \frac{|E||V|}{|Z|} \sin(\delta) \quad (1.12)$$

$$Q_{3\phi} = 3 \frac{|V|}{|Z|} (|E|\cos(\delta) - |V|) \quad (1.13)$$



$$\delta = \sin^{-1} \frac{P_{injected} |Z|}{3 * |E| |V|} \quad (1.14)$$

Consequently, a power factor controller can control  $\delta$  to maintain the power angle on bus 2 [49].

### 1.4.3 Reactive Power Control

As mentioned earlier in this thesis, inverter controllers control the reactive power output to maintain the power angle on the power grid. Given the angle reference, equation (1.13) determines the reactive power that should be delivered to the power grid. One way to control reactive power is to change the reactance by deploying a reactive compensation device.

The number of inverters within the system can be calculated according to the following equation:

$$\text{Numbers of inverters} = \frac{P_{PV}}{P_{\text{rated power of one inverter}}} \quad (1.15)$$

In figure (1.2), when a photovoltaic power station injects power into a power grid, the power grid voltage is not equal to the photovoltaic voltage due to the resistance and reactance of the transmission line. Equation (1.16) shows the injected power from two buses' voltage ( $U_{bus}, U_{PV}$ ) and transmission impedance ( $R + jX$ ).

$$S_{bus} = P_{bus} + jQ_{bus} = U_{bus} I_{line}^* = U_{bus} \frac{U_{PV} - U_{bus}}{(R + jX)^*} \quad (1.16)$$

Equation (1.17) shows the injected reactive power. Move the reactive power to the left-hand side and select the image part of the equation on the right-hand side.

$$Q_{bus} = \frac{U_{bus}U_{PV}^* - U_{bus}^2 - P_{bus}R}{X} \quad (1.17)$$

According to equation (1.17), the reactive power of the power grid is inversely proportional to the line reactance. Therefore, the reactive power injection of a bus can be controlled by changing the reactance of the line by using a compensator [54].

#### 1.4.4 Voltage Control

In figure (1.3), the power grid voltage( $V_2$ ) can be maintained by changing the transformer's turn ratio( $t_S, t_R$ ).

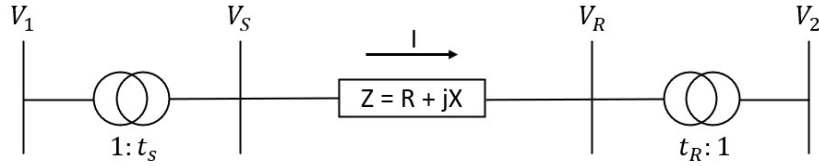


Figure 1.3: Two buses power grid

First, calculate the injected power( $S_2$ ) to determine the current( $I$ ). Equation (1.18) shows the injected power at the power grid bus.

$$S_2 = P_2 + jQ_2 = \bar{V}_R |I| \cos\theta + j\bar{V}_R |I| \sin\theta \quad (1.18)$$

Then, in equation (1.19), multiply the injected power( $S_2$ ) with the transmission line( $R+jX$ ) and extract the real part to find the voltage change on the transmission line.

$$\Delta V = \frac{RP_2 + XQ_2}{V_R} \quad (1.19)$$

Finally, in equation (1.20), use the ratio of transformers and the voltage change to find the relation between generator and power grid voltage. PV can control the generator voltage( $V_1$ ) to maintain the power grid voltage( $V_2$ ).

$$t_s V_1 = t_R V_2 + \frac{RP + XQ}{t_R V_2} \quad (1.20)$$

## Chapter 2

### Models Used for Simulation

In this thesis, three measurement-based inertia estimation methods are developed to estimate the virtual inertia from PMU measurements. Simulations, conducted in PowerWorld Simulator, are used to generate data that mimic the PMU measurements. In PowerWorld Simulator, dynamic models for synchronous generators and PVs are needed to analyze the transient stability of the system. This chapter details the dynamic models used in simulations.

#### 2.1 Synchronous Generator Model

Traditional synchronous generators are equipped with two types of controllers, i.e., governor and excitors, to regulate power grid frequency and voltage variations after a disturbance occurs. Governor controllers control the threshold of the sources of the input energy, such as steam, to accelerate a turbine's rotational speed. Excitors control the output voltage to reduce the risk of voltage collapse. According to equation (1.13), the voltage magnitude is regulated by the reactive power in a power system. Therefore, controlling the reactive output power can maintain the output voltage.

##### 2.1.1 Machine Model

This thesis uses a two-axis synchronous dynamic model to simulate synchronous generator machines. The machine model shows the process of controlling the output voltage and current. Since the generator is a two-axis synchronous generator, each pole can produce output voltage  $(E_q, E_d)$  and current  $(I_q, I_d)$ . According to the reactance  $(X_d)$  and transient reactance  $(X'_d)$  of

the generator model, an exciter sends voltage reference to regulate the output voltage.

The machine model shows the process of controlling output voltage( $E_q$ ) in figure (2.1). The input comes from a feedback signal( $E_{fd}$ ) of an exciter model, which provides the reference voltage value. The error between the generator voltage and reference passes through an integrator block( $\frac{1}{T_d s}$ ) to regulate the output voltage.

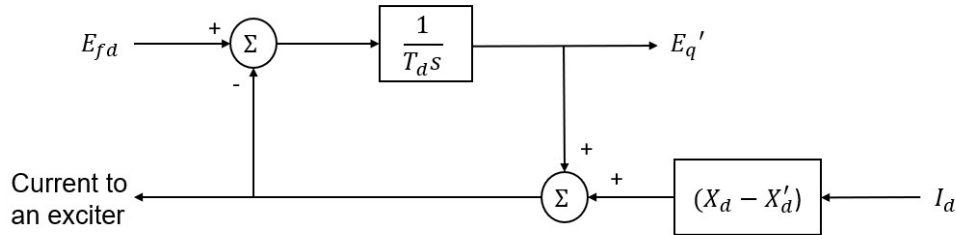


Figure 2.1: Machine Model [56]

### 2.1.2 Exciter Model

In 1968, the excitation system subcommittee(the Power Generation Committee of IEEE Power Group) [55] proposed an exciter model. The model shown in figure (2.2), uses the terminal voltage ( $V_T$ ) as the input and compares the terminal voltage with the voltage reference value ( $V_{ref}, Other\ signal$ ) to provide the field voltage ( $E_{fd}$ ) to the machine model. The voltage error is an input to a first-order lag block, which includes an error gain ( $K_{gain}$ ) and a time delay( $T_A$ ), to regulate the voltage. However, a generator cannot provide unlimited voltage. The generator voltage is limited by a limiter determined by ( $V_{max}, V_{min}$ ) range. The output signal depends on the voltage dynamic regions: linear dynamic region or saturation region. The saturation function will be the additional feedback to influence the input of the phase compensator ( $\frac{1}{K_g + sT_g}$ ). Additionally, the damping factor on a DC motor influences the error voltage [56].

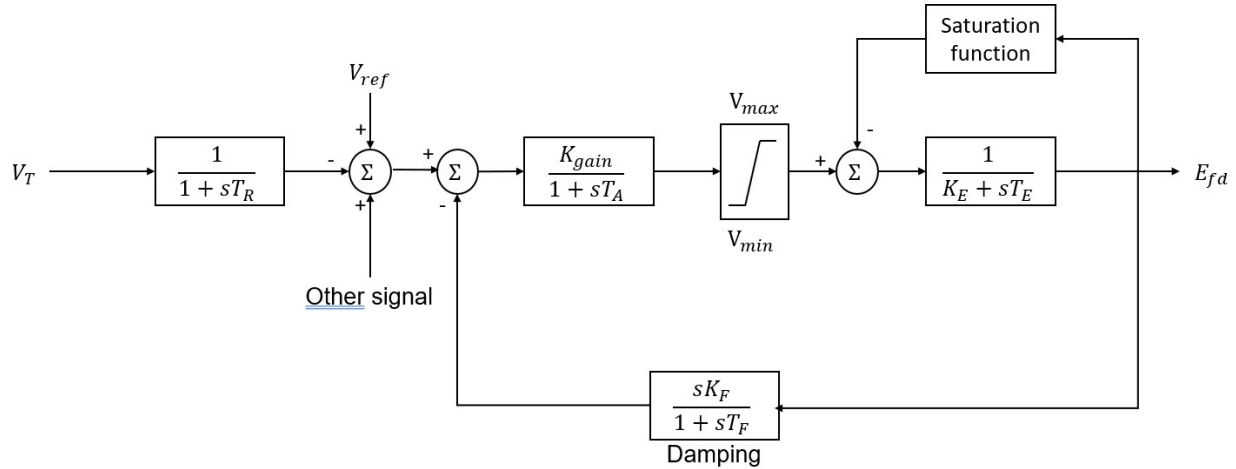


Figure 2.2: IEEE T1 exciter model [57]

### 2.1.3 Governor Model

A turbine drops the rotational velocity to generate additional energy to compensate for the electrical power imbalance when the total generated output power decreases. In figure (2.3) [57], a governor model detects the frequency change ( $\Delta\omega$ ) to control the output mechanical power ( $P_{mech}$ ). The real power reference ( $P_{ref}$ ) comes from the dynamic model on a synchronous generator. The mechanical power increases to compensate for the power imbalance. The governor input is limited to prevent excessive turbine rotations. Therefore, the model uses phase compensators and lead-lag controllers to slow down the output frequency changes. The real output power ( $P_{mech}$ ) comes from the difference between a series of blocks and the production of damping factor ( $D$ ) with frequency changes ( $\Delta\omega$ ). The series controllers include a permanent droop constant ( $R$ ), time delay ( $\frac{1}{1+sT_1}$ ), and a lead-lag compensator ( $\frac{1+sT_2}{1+sT_3}$ ) [58].

## 2.2 Model of the Renewable Generator

The Western Electricity Coordination Commission (WECC) developed the first generation wind turbine model in 2008 to simulate wind turbines [59]. In 2010, WECC developed the second-generation generator model, which can simulate wind turbines and photovoltaic

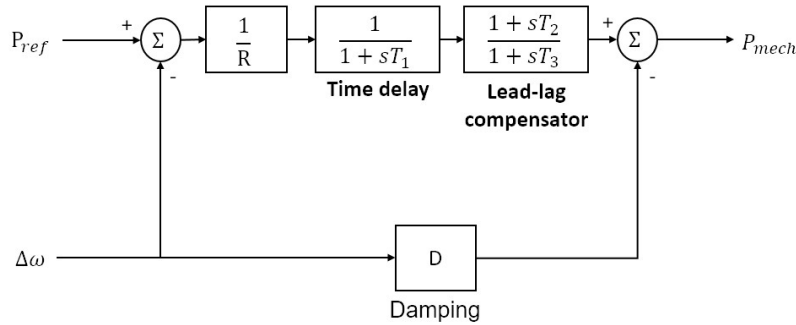


Figure 2.3: TGOV1 Governor Model [58]

power generation [59]. In this thesis, the second generation model is used to simulate large photovoltaic generators, excluding the battery model [59].

Wind power generation and solar power generation are modeled in a similar manner in simulations. They need inverters to convert DC power to AC power. When a wind turbine rotates, the wind turbine is unstable because of changes in wind speed. In order to maintain the output power, an inverter is needed to transfer the input source to a stable output source. Similarly, an inverter model is necessary to simulate solar energy in the PowerWorld Simulator. Large renewable generators are in need of controllers to respond to grid changes, such as reactive power control, voltage control, or power factor control. Before a renewable generator can inject power into the grid, a machine model is needed to control the output voltage, such as a frequency converter [60].

This thesis uses two models to simulate large photovoltaic generators: the REGCA model [60] for the machine model and the REECA model for the electrical model. The machine model receives current commands from the electrical model to determine how much power should be injected into the grid. Meanwhile, the machine model should manage the output voltage to prevent damage to the equipment. When the bus voltage is high, the machine model will reduce the reactive power to adjust the bus voltages. In figure (2.4), the machine model

has grid constraints to allow renewable generators to operate in safe areas, such as network boundaries and voltage limits [60].

The electrical model depends on different controls, such as reactive power control, to send current commands to the machine model. The electrical input can be a factory controller or a given constant value. Unlike a large-scale PV, a distributed PV does not contain an inverter controller to regulate parameters [61].

### **2.2.1 Wind Generators Model**

There are several models of wind turbines in PowerWorld Simulator, including machine, electrical, mechanical, and pitch controllers. PowerWorld Simulator has eight types of wind turbines for the first generation and four for the second generation. Unlike the first-generation models, some second-generation models have factory controllers to regulate the power grid [62].

The structure of the wind turbine model includes a pseudo-governor model, a wind turbine model, and a generator model. The pseudo-governor model receives electrical power from the generator model and turbine speed from the turbine model and sends mechanical power to the turbine model. The wind turbine model also receives electrical power from the generator model and mechanical power from the pseudo-governor model to determine the turbine speed. Finally, the generator model depends on the speed of the turbine to inject complex power into the grid—standard wind models from type 1 to type 4 [62].

### **2.2.2 Photovoltaic Model**

In contrast to synchronous generators, PV generators do not have governor and exciter controllers. In addition, photovoltaic power generation generates low-voltage DC, which cannot be directly injected into the grid. Therefore, PV systems are equipped with a two-stage power conversion for proper integration into the grid. Large PV plants need to control output



parameters to maintain stability. This thesis uses the REGCA model as the photovoltaic machine model and the REECA model as the electrical model [61].

The REGCA model, in figure (2.4), simulates a generator with a converter. According to the voltage of the bus (*voltage function*) and the current commands of the electrical model ( $I_q, I_p$ ), the machine model controls the injected complex power. The output complex power depends on the current command of the electrical model. The reactive output power depends on the network boundary and the electrical model command. If the bus voltage is too high, to prevent damage to the equipment, the machine uses the maximum voltage to determine the reactive output power [61].

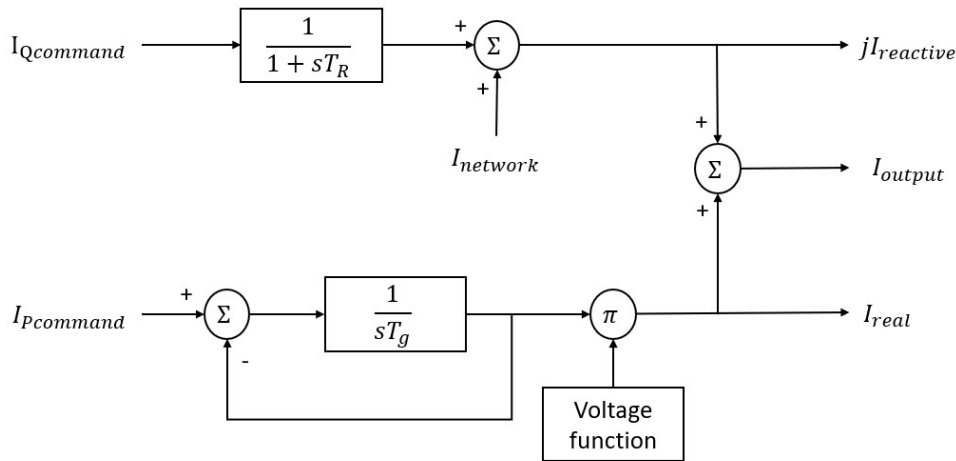


Figure 2.4: PV Machine Model [59]

When the voltage drops, the electrical model increases the reactive current command to provide more reactive power. However, a machine model limits the reactive current command based on the reactive power capacity of a generator. For limited conditions, a machine model shall increase or decrease the output reactive current according to the bus voltage: the output reactive current decreases when the bus voltage exceeds the pre-fault value. However, if a bus voltage exceeds the maximum limit threshold, the reactive output power is limited.

A machine model receives current commands as offsets and multiples and has low voltage active current management gain for real output power. When a bus voltage is lower than the pre-fault value, a machine model will reduce the real output power and increase the reactive output power. However, if a bus voltage is below the minimum threshold, a machine model provides the minimum real output power to maintain the real power injection of the grid [61].

The REECB model is an electrical model of an inverter. Unlike REECC, REECB has no energy storage function. The electrical signal sends the current command to the machine model according to the bus status. This model has three types of controllers: power factor controller, reactive power controller, and voltage controller. The theory of these controllers will discuss in the next section. The electrical model can select the type of controller applicable to renewable generators. The electrical model receives electrical power from the generator for power factor control to generate reactive current commands. Alternatively, the model uses the reactive power of the generator to determine the reactive current command to achieve voltage control. Reactive power control depends on the terminal voltage to determine the output current command (if applicable). In addition, the current command depends on the factory controller or the initialization constant with the bus voltage. The REECC model uses additional battery models for real power current commands [61].

The input of the power factor controller comes from the power system. Large-scale photovoltaic power generation must respond to the power system, so the input is electrical power with a power factor, and the output is reactive power. Distributed PV only provides constant reactive power, so no power factor control exists. If photovoltaics has power factor control, the controller will determine the reactive output power according to the electric power with power factor. Otherwise, distributed photovoltaics have no power factor control and provide constant reactive power.

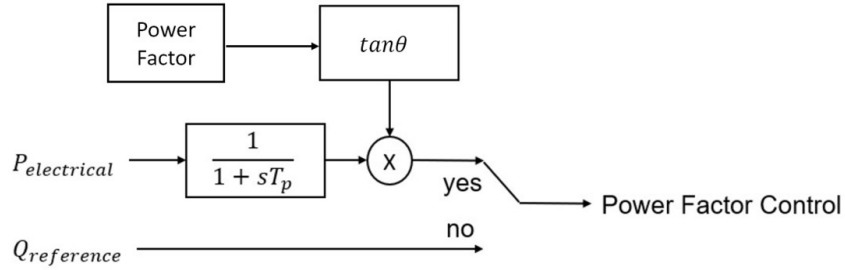


Figure 2.5: Power factor control [59]

In order to reduce the error of reactive power reference, the electrical model uses a proportional-integral controller (PI controller) [61]. In a PI controller, input and output are proportional. The integral block can reduce the error. The controller uses two limits to limit the reactive output power and voltage in contact with unsafe areas. Then, the controller uses the current parameters to obtain the error between reference values and uses the PI controller to reduce the error [61].

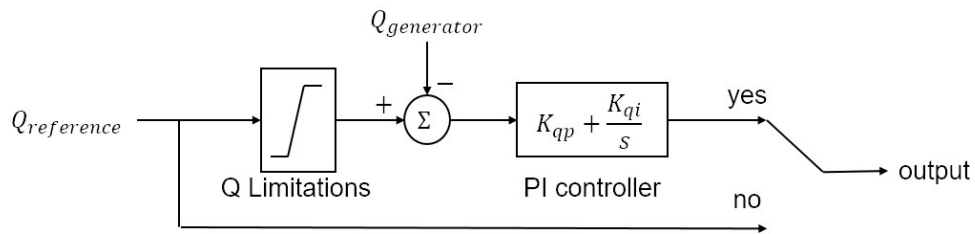


Figure 2.6: Reactive power controller [59]

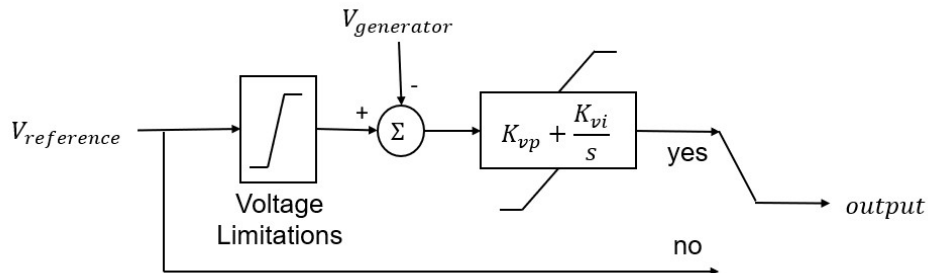


Figure 2.7: Voltage controller [59]

Unlike large renewable generators, some photovoltaics are small distributed generators.

Because of its small scale, this model does not need controllers as complex as other models. PowerWorld Simulator provides a model, PVD1, for simulating distributed photovoltaic generators. The model can provide a constant or reactive power factor for the power grid but cannot maintain the bus voltage [61].

## 2.3 PowerWorld Simulation

The thesis used IEEE 37 bus grid, in figure (2.8), to simulate the impact of photovoltaics in the PowerWorld Simulator. The thesis creates disturbances in one second and clean disturbances in five seconds. This interference simulates the influence of weather conditions, and PV reduces the real output power to a specific value. The power grid loses power during the transient, and the frequency decreases. After five seconds, the interference disappears, the current increases, and the frequency suddenly increases. The Orange generators represent photovoltaic, while the white generators represent synchronous generators.

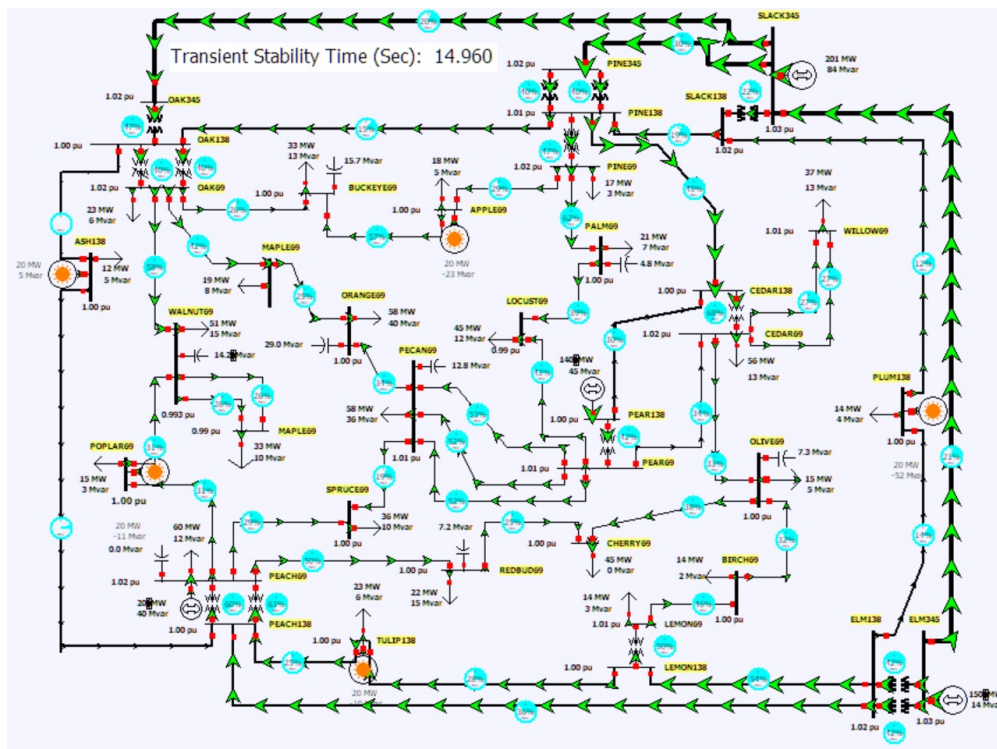


Figure 2.8: IEEE 37-buses power grid

In addition, the weather conditions may differ from those in other regions, so some photovoltaic equipment will not reduce the output power during the disturbance. The thesis created 700 weather conditions to simulate all possible weather conditions, each of which can provide 2000 PMU data for each parameter, such as frequency, voltage, and generator power.

### 2.3.1 The Primary Control Stage

When a disturbance occurs, photovoltaic frequency change is more severe than synchronous generator frequency change in figure (2.9). The reason is that the synchronous generator has a turbine to compensate for the frequency deviation. However, photovoltaic has no rotating unit, and its inverter cannot immediately respond to interference. After seven cycles, the governor and electrical model react to the sudden drop in frequency and stop the sudden drop in frequency.

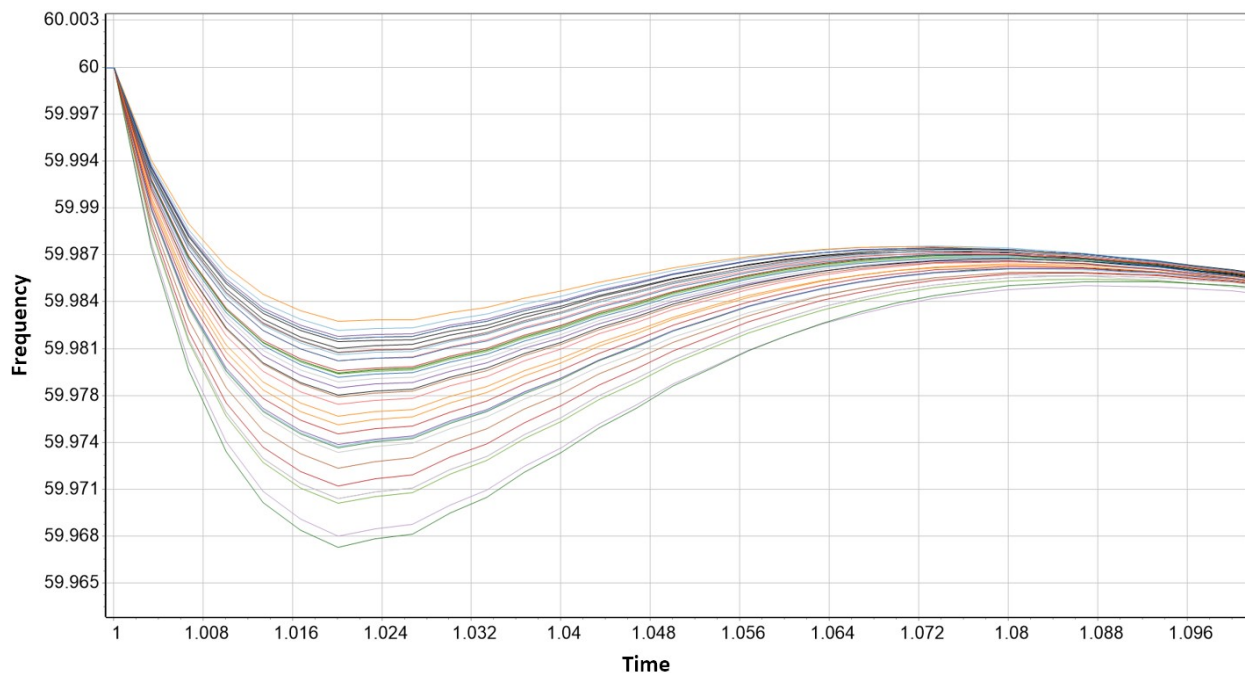


Figure 2.9: The moment when a disturbance happens.

The PV penetration comes from equation (2.1), the total PV power divided into the load

demand. In table (2.1), the thesis replaced a 25 megawatts synchronous generators with five distributed renewable generators, each of which can provide 5 MW. In the second and third scenarios, the thesis replaced 10 percent of synchronous generators with five distributed renewable generators, each of which can provide 10 MW. In the four scenarios, the thesis replaced 40 percent of synchronous generators with five distributed renewable generators, each of which can provide 33 MW. In the five scenarios, the thesis replaced 50 percent of synchronous generators with five distributed renewable generators, each of which can provide 63 MW. When interference occurs, all photovoltaics will reduce their real output power. This table shows the lowest frequency point of the main control phase. At this stage, only synchronous generators can release the inertia of the turbine, and they can reduce the frequency drop. However, photovoltaics cannot react to interference immediately; the Frequency drop is more severe than synchronous generators.

$$Penetration = \frac{PV\ Power}{Load\ Demand} \quad (2.1)$$

Table 2.1: Lowest frequency points(replace one synchronous generator)

Number	PV	Synchronous generators
1	59.974	59.983
2	59.973	59.983
3	59.972	59.982
4	59.969	59.979
5	59.968	59.976

When the penetration of renewable energy increases to 10%, in table (2.2), the thesis retired two synchronous generators, providing 50 megawatts of power to observe the impact. The lowest frequency point is less than the former case because the total inertia from synchronization is reduced.

Table 2.2: Lowest frequency points(replace two synchronous generators)

Number	PV	Synchronous generators
1	59.966	59.9794
2	59.966	59.9794
3	59.966	59.9776
4	59.964	59.9773
5	59.963	Retired

Table 2.3: Lowest frequency points(replace three synchronous generators)

Number	PV	Synchronous generators
1	59.574	59.675
2	59.552	59.674
3	59.545	59.671
4	59.507	Retired
5	59.498	Retired

When renewable energy penetration increases to 40%, in table (2.3), this thesis replaces three synchronous generators, which provide 150 mega watts. The frequency drops more severely in the primary control stage.

The synchronous generator must continue to effectively reduce the frequency during the main control phase. As a result, replacing more synchronous generators with PVs will reduce the capacity of total inertia. The lowest frequency will be lower while add more PV penetration.

### 2.3.2 PV Regulation

During the primary control phase, the governor and inverter controller begin to regulate the grid. Different types of photovoltaics will have different performances in the primary control stage. For example, in figure (2.10), discrete PV does not have a inverter controller. Distributed photovoltaics do not regulate the power grid when a disturbance happens. Only synchronous generators use controllers to regulate the abnormal power grid. Therefore, frequency recovery time will be longer than PV with inverter control.

Large-scale photovoltaic cells, in figure (2.11), can provide reactive power control, and the

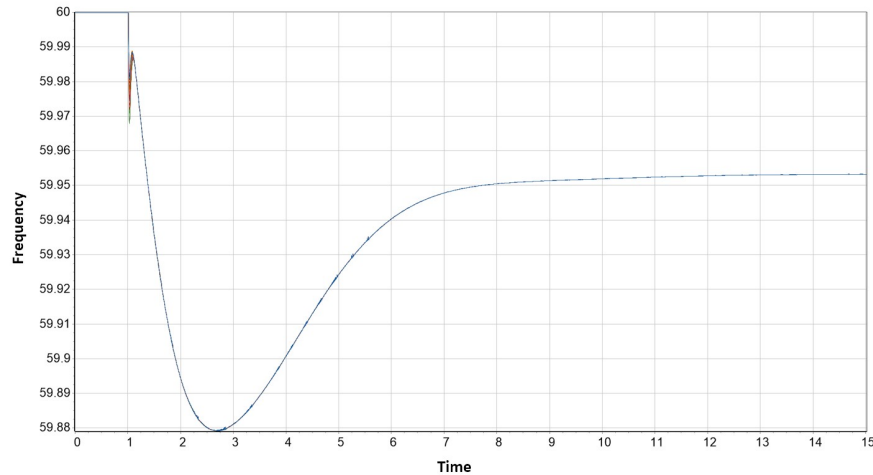


Figure 2.10: Frequency curves without inverter control

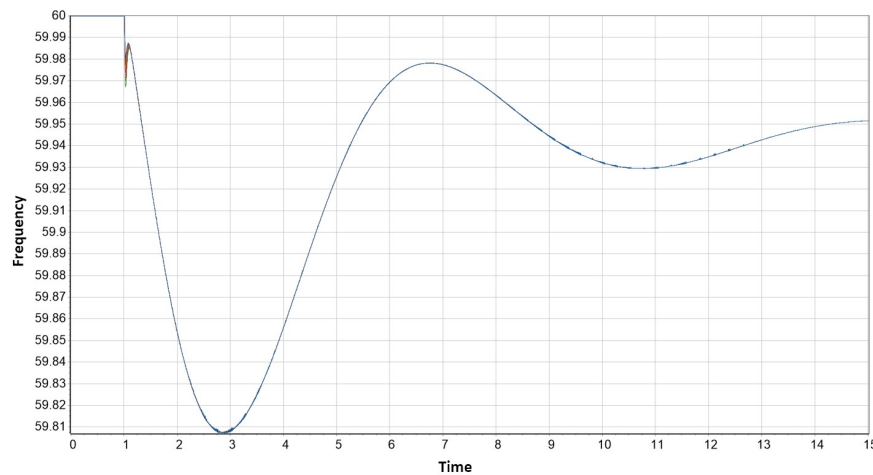


Figure 2.11: Frequency curves with inverter control

frequency curve can recover faster than discrete photovoltaic cells. When a disturbance occurs at one second, the real power of a photovoltaic generator decreases. The inverter controller cannot respond immediately to disturbances, and therefore, the frequency drops suddenly before the PV systems start compensating for power imbalance and adjusting the grid.

## 2.4 PMU Measurement Data

This thesis uses PowerWorld Simulator to generate PMU measurement. In the software, an IEEE 37-buses power grid with different PV levels is built to generate PMU measurement.



Each bus can provide several parameters, including frequency, rate of change of frequency, voltage, phase angle, real power, and reactive power. Moreover, according to the output power on each PV, changing the output power and running the transient stability analysis to simulate seven hundred weather conditions. As a result, the PMU measurement includes seven hundred weather conditions data, and each weather data includes 37-buses information. Each bus information has two thousand time series data for fifteen seconds. Furthermore, PMU measurement is randomly divided into two categories, training data(70%) and testing data(30%), to observe the accuracy of the three inertia estimation methods.

## Chapter 3

### Inertia Estimation

This thesis proposes three measurement-based methods to estimate the virtual inertia of the systems with high levels of PV systems. The first method, i.e., the Symbolic Aggregate Approximation (SAX) [51], estimates the inertia from historical PMU measurements and classifies real-time PMU measurements into groups to estimate the virtual inertia. Two other methods, namely Minimum Enclosing Ellipsoid (MVEE) with Gradient Descent Machine Learning and Back Propagation Neural Network (BNN), are also used to estimate the virtual inertia, and their performance is compared with SAX.

#### 3.1 Symbolic Aggregate Approximation

SAX method estimates the virtual inertia from large-scale PMU measurements. The input features, in figure (3.1), include parameters in all buses, such as frequency and electrical power. Each PMU time-series measurement is divided into several time windows, and a K-nearest Neighbor Algorithm classifies a real-time PMU measurement and finds the most relevant data in the data pool to estimate the virtual inertia.

In this thesis, SAX converts each PMU measurement into two hundred time windows, in figure (3.2), and each time window contains eight input features in 0.06 seconds. The input features include frequency, the rate of frequency change, real power, real power deviation, voltage, voltage change, phase angle, and phase angle acceleration. Adding eight input

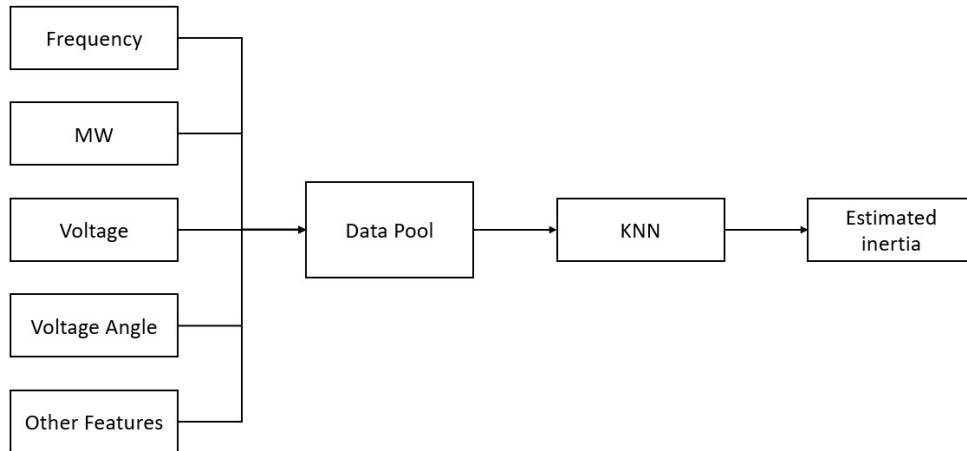


Figure 3.1: Illustration of SAX

features can increase the estimated accuracy with short time windows. Also, taking the average of measurement data in each window can reduce the complexity of the data pool. Data compression reduces the complexity of building a data pool compared to other methods.

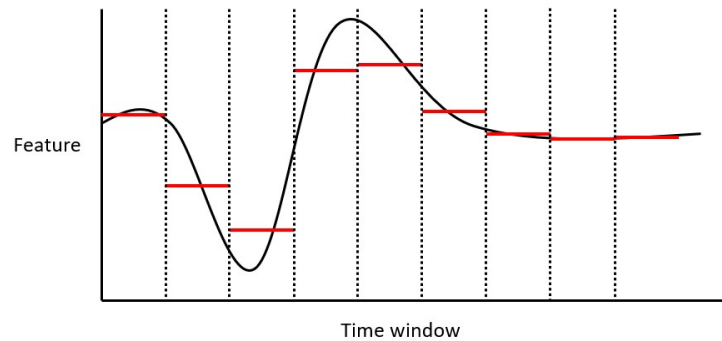


Figure 3.2: Illustration of dividing PMU measurement into time windows

After a data pool is created, it is used to estimate the virtual inertia of a power system from real-time PMU measurements. This thesis uses K-nearest Neighbor (KNN) algorithm to classify real-time data in a data pool. The difference in parameters between real-time and historical data are used to classify similar parameters in order to compute the label inertia. Select the K numbers of the nearest data to calculate virtual inertia using classification or regression functions.

### 3.1.1 K-nearest Neighbors Algorithm

The KNN algorithm selects  $K$  data points with parameters similar to the real-time PMU data. For example, in figure (3.4), the white circle represents the real-time PMU data needed to estimate the virtual inertia. The orange and blue circles represent historical data in a data pool. Only the orange circle is considered in the KNN model when  $K$  equals one. For inertia classification estimation, the label of the orange circle equals to the estimated inertia. Moreover, when  $k$  is two, two blue and one orange circle are considered. The estimation of inertia will use a classification or regression function to determine the estimated inertia from their label inertia (equation (1.7)). The classification function selects the label inertia of the highest density group as the virtual inertia. The regression function takes the average of all label inertia as an estimated output. The advantage of increasing  $k$  is to avoid extreme PMU measurement due to numerical problems. For example, when a disturbance occurs, frequency suddenly drops and causes the label inertia to become an extreme value (equation (1.7)). Therefore, even though a data pool has data points similar to real-time PMU data, the estimated inertia may have a significant error.

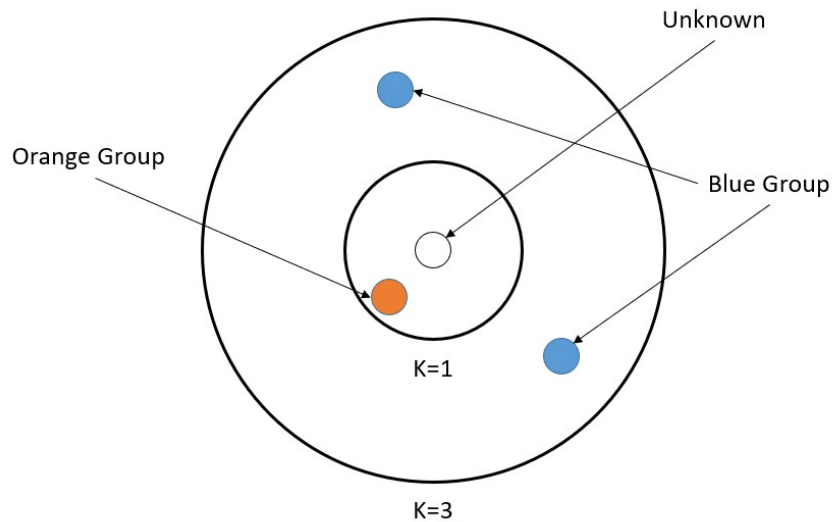


Figure 3.3: K-nearest Neighbor algorithm model

### 3.1.2 Inertia estimation

Two inertia estimation functions are used to estimate the virtual inertia. The regression function in equation (3.1) takes the average of the label inertia from the selected data. The classification function uses Euclidean Distance to take the label inertia from the highest-density group of data points. Figure (3.4) shows the root mean square error between the estimated inertia (equation (1.6)) and the label inertia. When  $K$  is between 4 and 6, the regression function more accurately estimates the inertia compared to the classification function. When  $K$  exceeds six, the classification computes a constant error because the function selects the same group in a data set. However, the regression function has higher errors when  $K$  is more than seven because the function selects some extreme label inertia and computes the output.

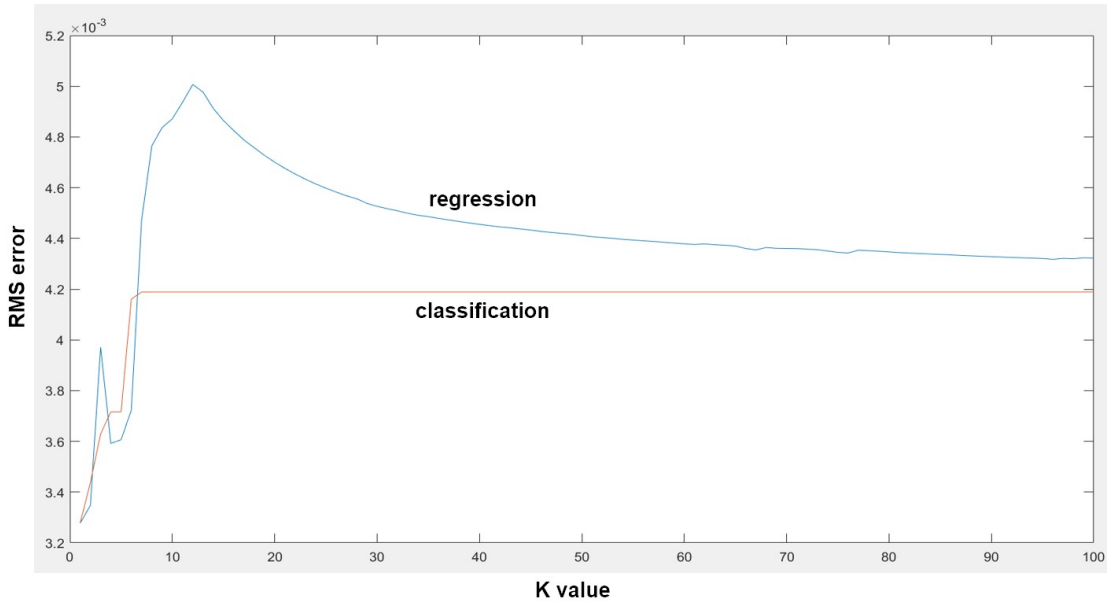


Figure 3.4: RMS error for regression and classification functions with different  $K$  values

$$Estimated\ inertia = \frac{1}{K} \sum_{i=1}^K Label\ inertia_i \quad (3.1)$$

## 3.2 Other Methods

This thesis uses two inertia estimation methods to compare the accuracy of the estimated inertia with the inertia estimated with SAX. One method is Back Propagation Neural Network (BNN) [63], and the other method is Minimum Volume Enclosing Ellipsoid (MVEE) [24] with Gradient Descent Machine Learning.

### 3.2.1 Back Propagation Neural Network

A Back Propagation Neural Network, in figure (3.11), is a non-linear classification method based on machine learning. PMU historical measurement, which is a network input, includes frequency and electrical power changes. Based on the input features, BNN classifies the data into different groups. Therefore, a network can classify a real-time PMU measurement to estimate the virtual inertia of a data set. The most relevant group is determined, and the label inertia of the group results in the estimated inertia. Before training a network, the initial weight of branches must be adjusted to successfully classify the input features. A network computes the estimated output by an activation flow and uses the error between the target and the output to adjust the weight of the branches.

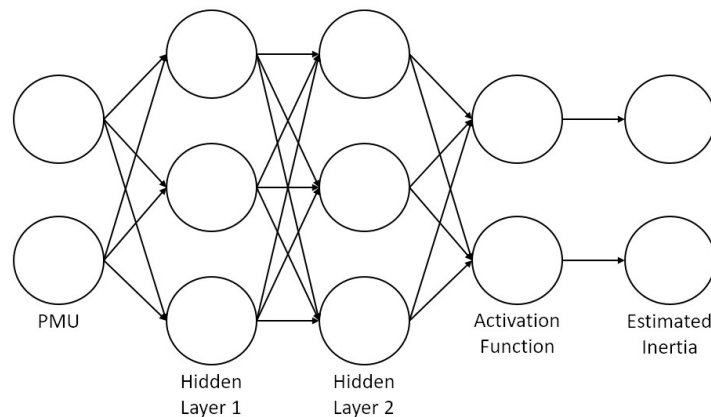


Figure 3.5: Illustration of a Back Propagation Neural Network

## Initial Setting

Before training, the initial setting of the weight of branches, as shown in figure (3.6), impacts the classification process. For an ideal distribution of input features, the relation between the loss function and the weights of the branches only has one optimal point, as shown with the red arrows (the classification line in figure (3.7)). However, the curve is not ideal for a real case, which increases the challenge of classifying input features. If all branches start at the same weight, the network only can classify input features into the same groups. Therefore, randomly selecting the initial settings avoids such problems, as shown with the purple and green arrows in figure (3.8).

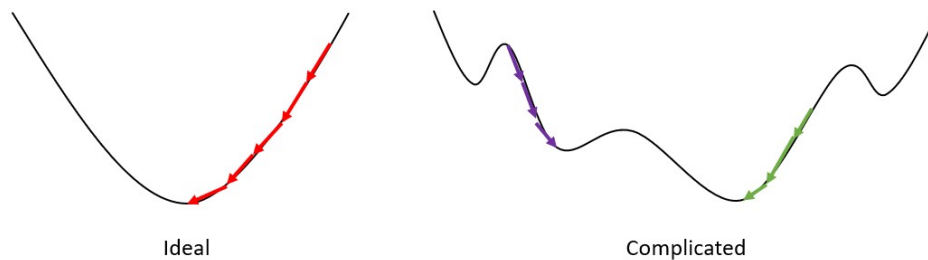


Figure 3.6: Illustration of the loss function and learning rate (Y: Loss function, X: weight values)

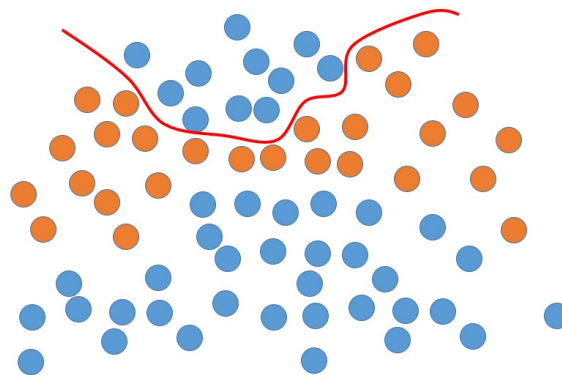


Figure 3.7: With a same initial weight of branches

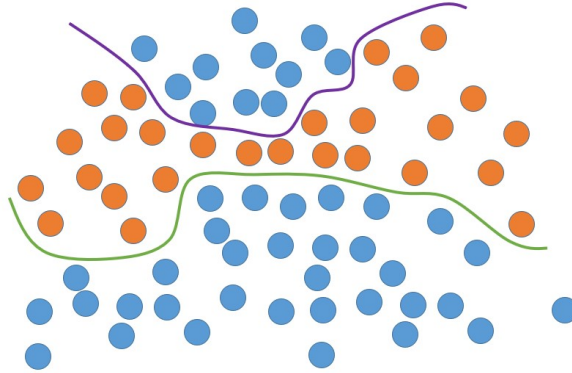


Figure 3.8: With a random initial weight of branches

## Classification Function

A network classifies input features from the PMU measurement. During the process, neurons classify input features using an activation function, such as the Sigmoid function (equation (3.2)). The input features ( $x$ ) of the activation function come from the PMU measurement or the output of the front layer.

$$\text{Sigmoid function} = \frac{1}{1 + e^{-x}} \quad (3.2)$$

## Bias

Adding bias can enhance the accuracy of inertia estimation. The gradient of the sigmoid function moves the position of the curve in figure (3.9) to classify the input features. Without adding bias, all curves pass through the same point (0,0.5), which reduces the efficiency of classifying the data. Therefore, adding bias can make the classification curve more flexible and effective.



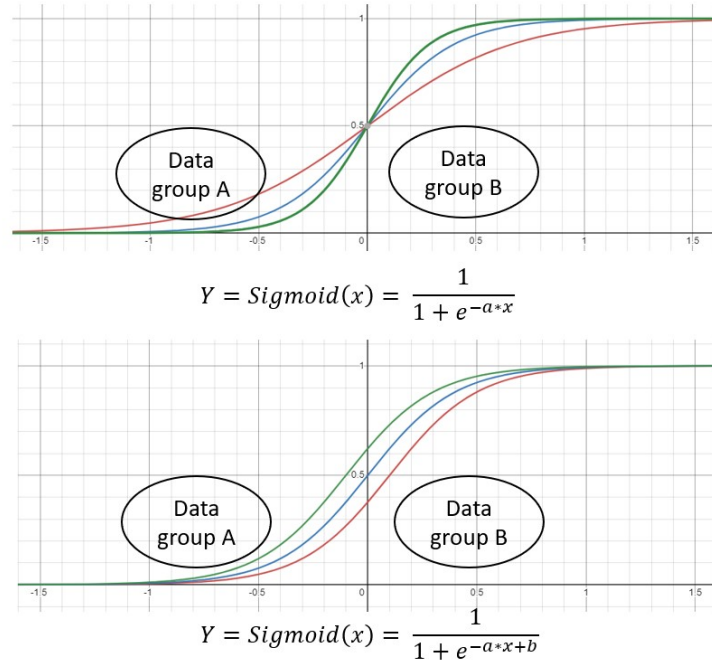


Figure 3.9: Illustration of the Sigmoid function

## Inertia Estimation

Figure (3.10) demonstrates the structure of a network. Equation (3.3) shows the process of calculating the estimated output. The input features ( $x_1, x_2$ ) come from the PMU measurements, and the weight of branches ( $wA, wB$ ) will be adjusted from the error flows. The Sigmoid function ( $\frac{1}{1+e^{-ax+b}}$ ) classifies the input features into different groups. The error flow adjusts  $a$  and  $b$  in the Sigmoid function, and bias ( $b$ ) assists the function in classifying inputs.

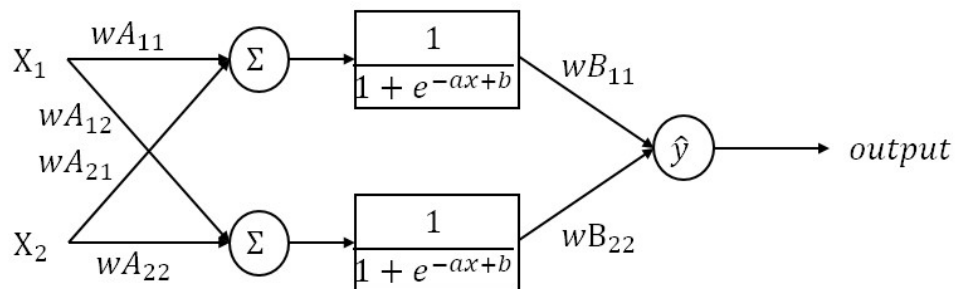


Figure 3.10: Illustration of a simple network

$$\hat{y} = WB_{11}Sigmoid(x_1WA_{11} + x_2WA_{21}) + WB_{22}Sigmoid(x_1WA_{12} + x_2WA_{22}) \quad (3.3)$$

After a network computes the estimated output ( $\hat{y}$ ), the estimated inertia may be far from the label inertia. Therefore, the root mean square error between the estimated output and the target is used to adjust the weight of branches to match the target. Therefore, the error of a neuron comes from the output RMS error and the differential Sigmoid function (equation (3.4)), as shown in equation (3.5).

$$Sigmoid'(x) = Sigmoid(x)(1 - Sigmoid(x)) \quad (3.4)$$

$$Neurons\ error = (\hat{y} - y)(1 - Sigmoid(x))Sigmoid(x) \quad (3.5)$$

Finally, the weight of the branches is adjusted from equation (3.6). In this thesis,  $\alpha$  is 0.5.

$$w_{new} = w_{old} - \alpha * \frac{\partial Neuron\ error}{\partial w_{old}} \quad (3.6)$$

With the selected activation and error flows, the network is fully trained by historical PMU measurements, and therefore the network can estimate the virtual inertia from a real-time PMU measurement by using activation flow only.

## Variation of the BNN Parameters

To determine which structure is suitable to estimate the inertia, figure (3.11) shows the relation between the number of neurons and the RMS error. As a result, the lowest RMS error is the best structure (194 neurons for each layer) to predict inertia.

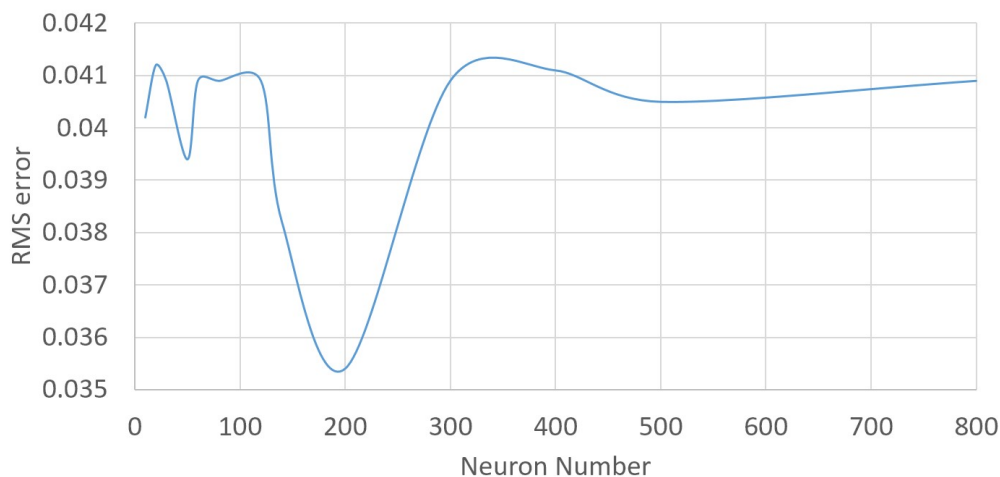


Figure 3.11: Illustration of the impact of the number of neurons in RMS error

### 3.2.2 Minimum Volume Enclosing Ellipsoid with a Gradient Descent Machine Learning Model

The Minimum Volume Enclosing Ellipsoid is a virtualization regression method, depending on the change of parameters. After a disturbance occurs, the parameters start to oscillate and influence stability. The input features include frequency, electrical power, and voltage. Three input features can be represented by a three-dimensional space, where each feature represents one axis. A MATLAB toolbox is used to draw a minimum volume enclosing ellipsoid and extract the volume as an output feature. The output feature will be the input source of a gradient descent machine learning algorithm to find a regression curve to estimate inertia.

To find the minimum volume ellipsoid, MATLAB tool(Minimum Volume Enclosing Ellipsoid on MatWorks) adjusts boundaries to find the minimum ellipsoid volume. Initially, the tool

randomly selects a center. Next, the boundary is adjusted according to the density of the data points, and another boundary is adjusted in other iterations. Finally, the minimum ellipsoid volume is found by gradient descent machine learning algorithm to estimate the virtual inertia.

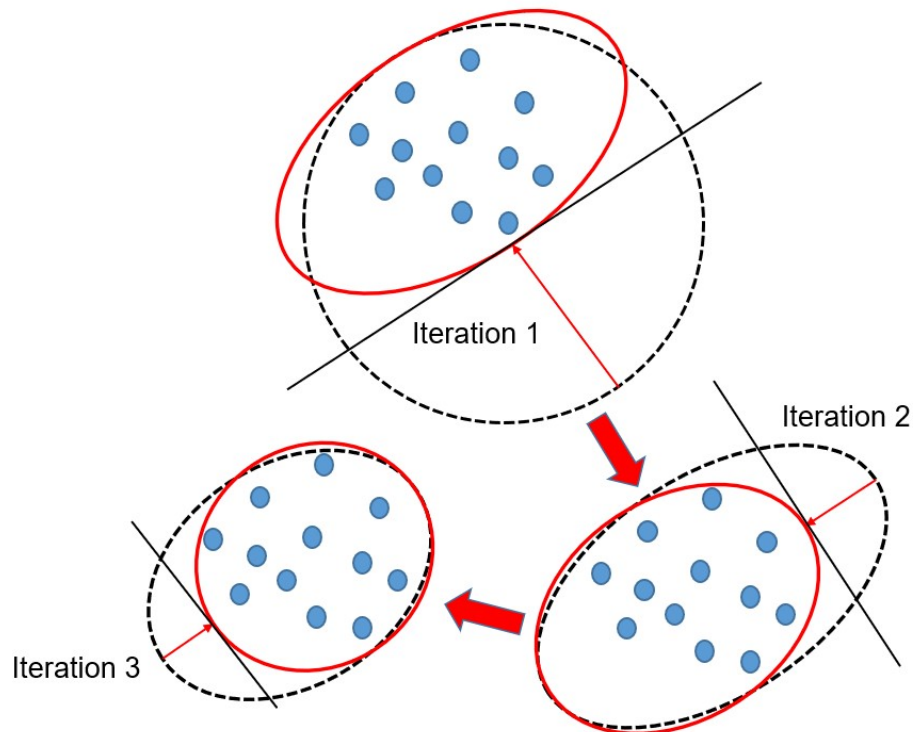


Figure 3.12: Illustration of finding a Minimum Volume Ellipsoid

## A Gradient Descent Machine Learning model

After finding the volume of ellipsoids from historical PMU measurements, a gradient descent machine-learning model calculates an optimal regression function between the volume of the ellipsoid and the label inertia. However, PMU measurements have extreme data, such as a sudden frequency drop, when a disturbance occurs. Those extreme data cause an accuracy problem for the regression function to estimate inertia. Therefore, a gradient descent machine learning can adjust the weight of different regression orders to reduce the influence of extreme data. The estimated inertia ( $\hat{y}$ ) comes from the function of ellipsoid volume ( $x$ ) in equation

(3.13).

$$\hat{y} = a + bx + cx^2 + dx^3 \quad (3.7)$$

The machine learning model adjust parameters from equations (3.9) to (3.12) to reduce errors depending on the loss function, equation (3.8). The learning rate  $\alpha$  is 0.8 in this thesis.

$$Loss\ function = \frac{1}{N} \sum_{i=1}^N (\hat{y} - y)^2 \quad (3.8)$$

$$a_{new} = a_{old} - \alpha * \frac{\partial Loss}{\partial a} = a_{old} - \alpha * (a + bx + cx^2 + dx^3) \quad (3.9)$$

$$b_{new} = b_{old} - \alpha * \frac{\partial Loss}{\partial b} = b_{old} - \alpha * ((a + bx + cx^2 + dx^3)x) \quad (3.10)$$

$$c_{new} = c_{old} - \alpha * \frac{\partial Loss}{\partial c} = c_{old} - \alpha * ((a + bx + cx^2 + dx^3)x^2) \quad (3.11)$$

$$d_{new} = d_{old} - \alpha * \frac{\partial Loss}{\partial d} = d_{old} - \alpha * ((a + bx + cx^2 + dx^3)x^3) \quad (3.12)$$

Finally, the result shows in equation (3.13) and figure (3.13). The estimated error increases

when volume increases because of extreme data points.

$$f(x) = 0.0013 - 0.1931x - 0.1946x^2 + 2.5039x^3 \quad (3.13)$$

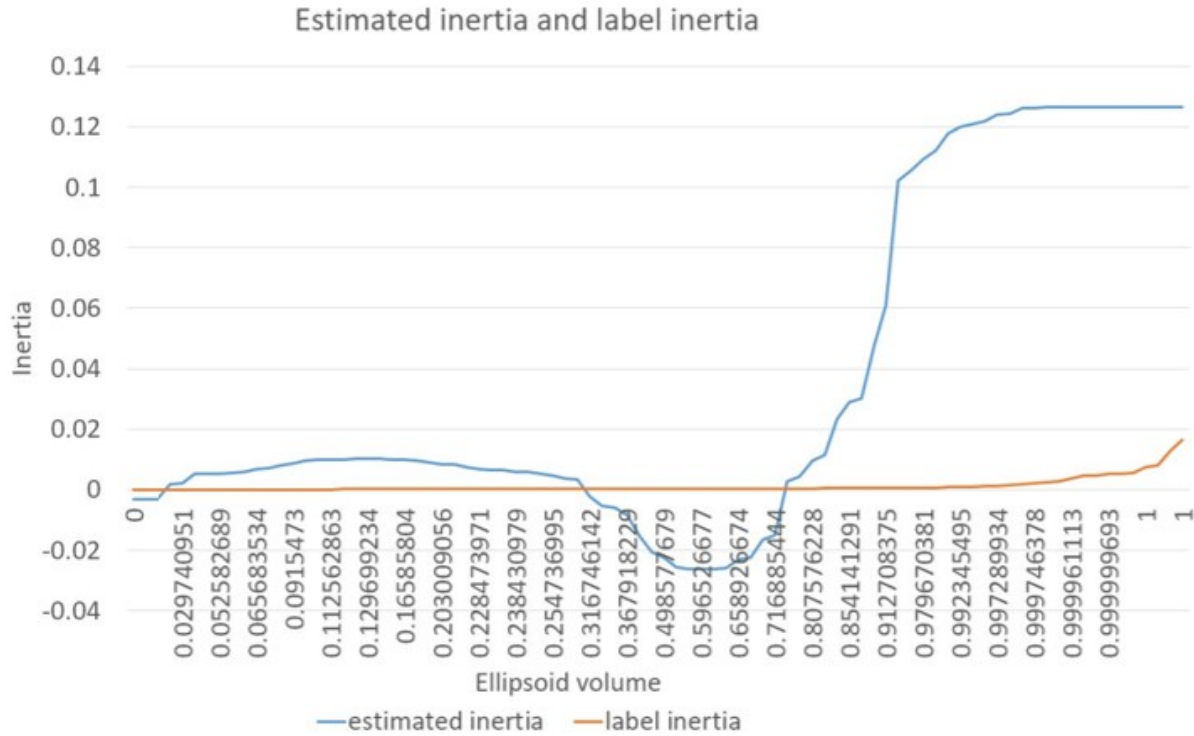


Figure 3.13: The error between the regression function and label inertia

This thesis builds different order regression functions and selects the best one to estimate the virtual inertia. The table shows that the third-order regression function is the best regression function.

Table 3.1: RMS error for different structures

Regression function order	PV1	PV2	PV3	PV4	PV5	average
1	0.098	0.0958	0.0939	0.0991	0.1034	0.098
2	0.2111	0.2176	0.2031	0.2277	0.2231	0.0137
3	0.0369	0.0403	0.0395	0.0394	0.0415	0.01196
4	2.15E5	2.19E5	2.113E5	2.363E5	2.314E5	2.226E5

## Chapter 4

### Sensitivity Analysis

This chapter shows the sensitivity of inertia estimation methods for different penetration of photovoltaic systems. Five scenarios simulate the impact of different PV penetration levels in an IEEE 37-buses power grid. The first scenario simulates replacing one 25 MW traditional synchronous generator with five PVs (3 percent penetration). The second scenario simulates replacing two synchronous generators, which provide 50 MW power, with five PV generators (10 percent penetration). Those PVs are placed in different locations, increasing their output power to match the total load. The third scenario is similar to the second scenario, but PVs have inverter controllers to regulate the power grid after disturbances occur. For the fourth and fifth scenarios, PVs provide large output power; therefore, PVs must have inverter controllers (according to IEEE 1547 standard) [47]. The fourth scenario simulates replacing three synchronous generators with photovoltaics, which provide 165 MW (40 percent penetration). The fifth scenario simulates replacing four synchronous generators with PVs, which provide 315 MW (50 percent penetration).

#### 4.1 Scenario 1: Distributed PV Penetration of 3%

The first scenario shows the estimated error of three inertia estimation methods. Figure (4.1) shows the root mean square error between the label and estimated inertia. The  $X$ -axis represents the number of time windows. Each represents 20 PMU measurements in 0.3 seconds. The  $Y$ -axis represents the average training error of the estimated inertia. All methods have significant errors at the 15th and 75th time windows due to extreme data

(sudden weather changes). Moreover, SAX-based classification and regression demonstrate a reasonable performance in estimating the inertia.

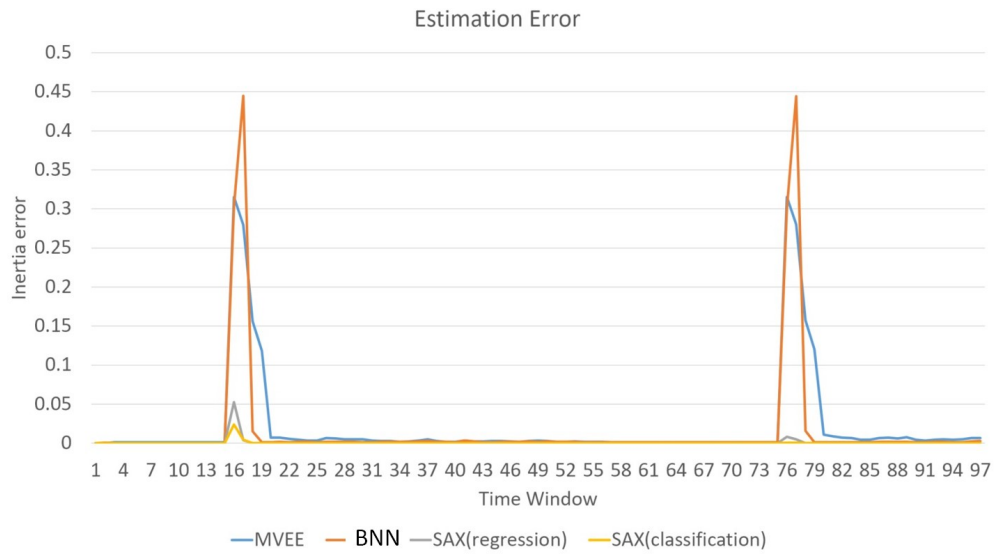


Figure 4.1: Illustration of estimated errors of the inertia estimation methods in the first scenario

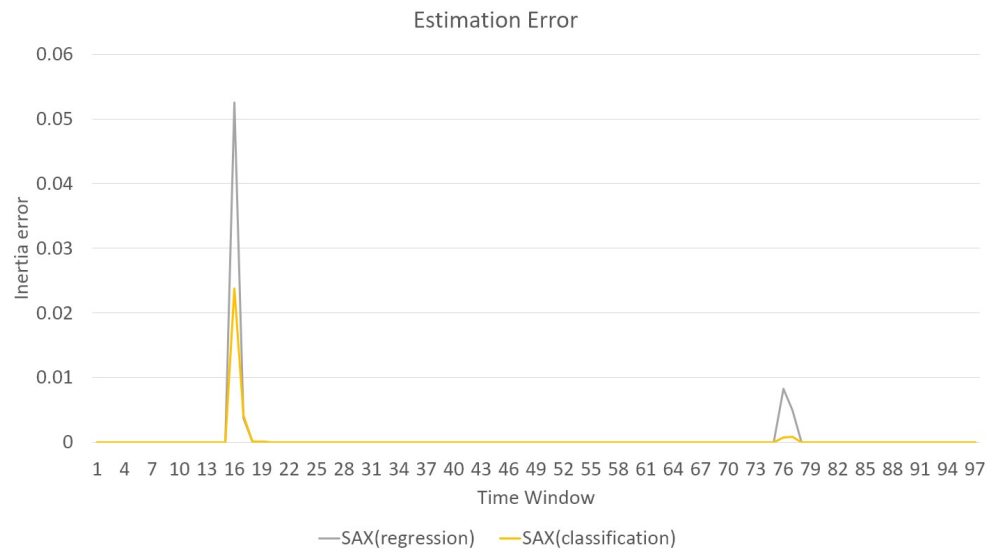


Figure 4.2: Illustration of errors of SAX in the first scenario

Table (4.1) shows the average RMS error of each PV unit within the system. Minimum Volume Enclosing Ellipsoid and BNN have higher average errors than SAX.



Table 4.1: RMSE for inertia estimation methods

	PV1	PV2	PV3	PV4	PV5	average
MVEE	0.021	0.024	0.023	0.0198	0.0213	0.0218
BNN	1.7E-2	1.7E-2	1.7E-2	1.7E-2	1.7E-2	1.7E-2
SAX(regression)	0.0007	0.0007	0.0007	0.0007	0.0007	0.0007
SAX(classification)	0.0003	0.0003	0.0003	0.0003	0.0003	0.0003

## 4.2 Scenario 2: Distributed PV penetration of 10%

The second scenario increases the PV penetration in the power grid. Figure (4.3) shows the root mean square error between the label and estimated inertia. Like the first scenario, the weather changes in the 15th and 75th time windows. Since distributed PVs do not have inverter controllers, parameters in a power grid are more uncontrollable than lower PV penetration because of less inertia storage.

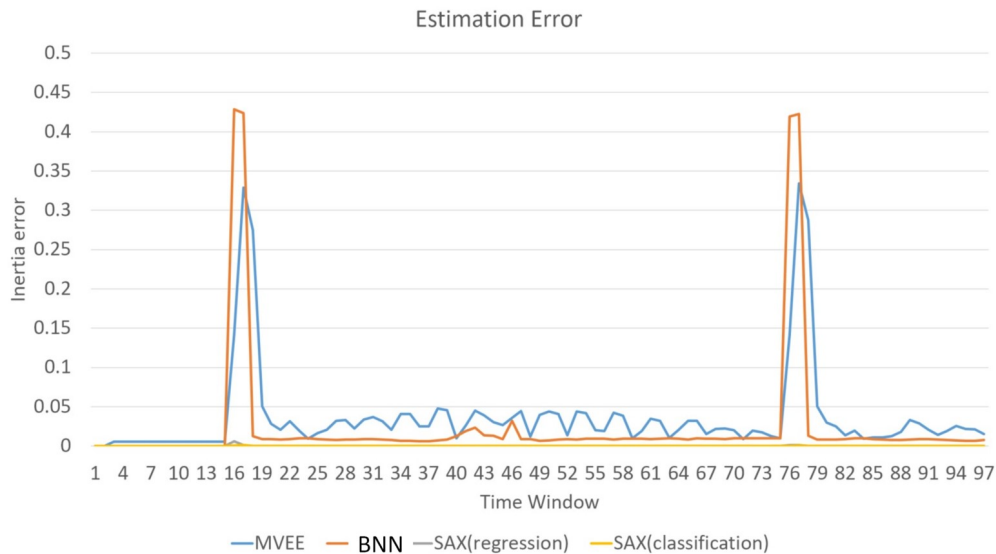


Figure 4.3: Illustration of estimated errors of inertia estimation methods in the second scenario

Table (4.2) shows the RMSE values for different PV units.

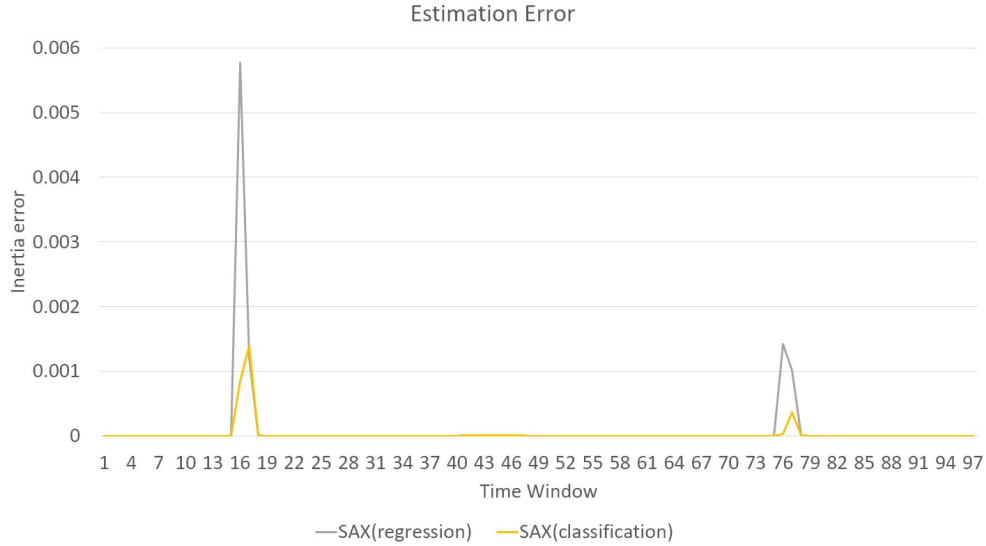


Figure 4.4: Illustration of errors of SAX in the second scenario

Table 4.2: RMSE for different inertia estimation approaches

	PV1	PV2	PV3	PV4	PV5	average
MVEE	0.0412	0.0400	0.0393	0.0392	0.0412	0.0402
BNN	2.5E-2	2.5E-2	2.5E-2	2.5E-2	2.5E-2	2.5E-2
SAX(regression)	9.73E-5	9.73E-5	9.73E-5	9.73E-5	9.73E-5	9.73E-5
SAX(classification)	2.76E-5	2.76E-5	2.759E-5	2.759E-5	2.759E-5	2.759E-5

### 4.3 Scenario 3: Large-scale PV penetration of 10%

The third scenario places large-scale PVs in the power grid and observes the impact on inertia estimation. Figure (4.5) shows the RMSE between the label and the estimated inertia. Unlike previous scenarios, PVs are large-scale generators, and they are equipped with inverter controllers to regulate the system parameters after disturbances occur. Table (4.3) shows the average RMSE values for different PV units. Compared to the second scenario, inertia estimation errors increase because of the inverter control, which controls output frequency and other parameters, such as the voltage. Therefore, the Minimum Volume Enclosing Ellipsoid method is challenged in calculating the regression function to estimate inertia due to extreme data. The BNN and SAX methods can estimate inertia more accurately because they can



#### 4.4 Scenario 4: Large-scale PV penetration of 40%

The fourth scenario also places large-scale PVs to replace synchronous generators. Figure (4.7) shows the estimated errors for inertia estimation methods.

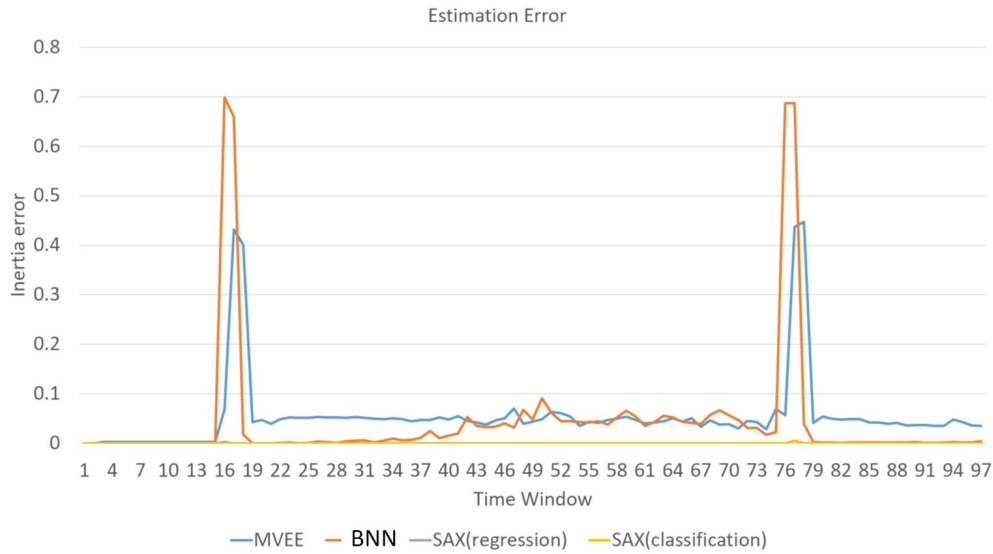


Figure 4.7: Illustration of estimated errors of inertia estimation methods in the fourth scenario

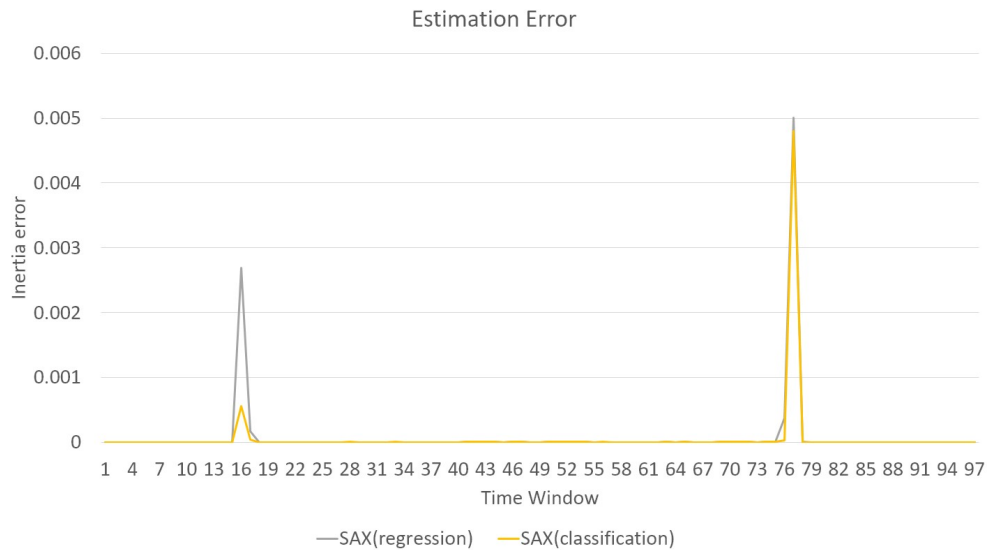


Figure 4.8: Illustration of errors of SAX in the fourth scenario

Table (4.4) shows the average RMSE values for different PV units. For the Minimum Volume Enclosing Ellipsoid and BNN methods, the errors increase due to the fact that the oscillation

of large parameters results in extreme data. The Minimum Volume Enclosing Ellipsoid method cannot find a fitting regression function to avoid extreme data, and BNN cannot classify those data into correct groups. However, the developed SAX method results in an acceptable classification performance because it can classify a real-time data into correct group.

Table 4.4: RMSE for different inertia estimation approaches

	PV1	PV2	PV3	PV4	PV5	average
MVEE	0.0538	0.047	0.046	0.046	0.042	0.0470
BNN	4.53E-2	4.53E-2	4.53E-2	4.53E-2	4.53E-2	4.53E-2
SAX(regression)	8.35E-5	8.35E-5	8.35E-5	8.35E-5	8.35E-5	8.35E-5
SAX(classification)	5.56E-5	5.56E-5	5.56E-5	5.56E-5	5.56E-5	5.56E-5

## 4.5 Scenario 5: Large-scale PV penetration of 50%

The fifth scenario simulates replacing synchronous generators with large-scale PVs. Figure (4.9) shows the estimated errors for inertia estimation methods, and figure (4.10) further demonstrates the errors from the SAX method.

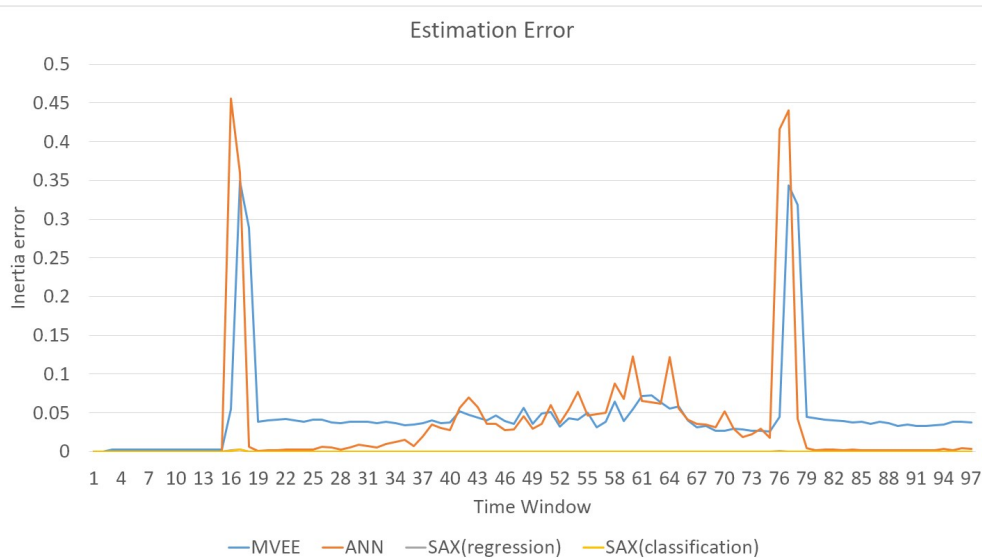


Figure 4.9: Illustration of estimated errors of inertia estimation methods in the fifth scenario

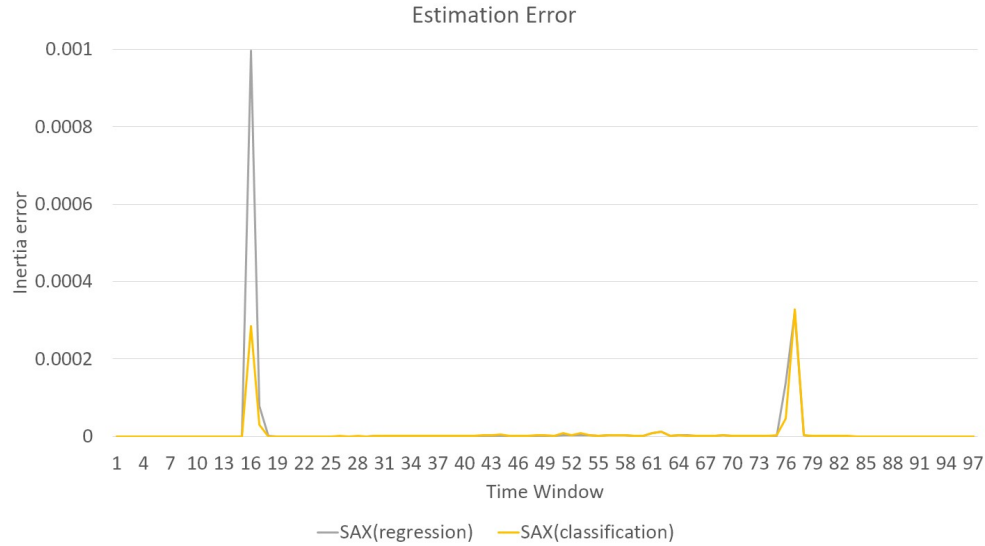


Figure 4.10: Illustration of errors of SAX in the fifth scenario

Similar to the fourth scenario, in table (4.5), errors from Minimum Volume Enclosing Ellipsoid and Back Propagation Neural Network are larger than Symbolic Aggregate Approximation.

Table 4.5: RMSE for different inertia estimation approaches

	PV1	PV2	PV3	PV4	PV5	average
MVEE	0.0463	0.047	0.048	0.045	0.046	0.0465
BNN	3.83E-5	4.38E-2	4.50E-2	3.92E-2	4.31E-2	3.59E-2
SAX(regression)	4.023E-5	9.63E-6	1.554E-5	1.601E-5	1.671E-5	3.696E-5
SAX(classification)	3.131E-5	4.90E-6	9.44E-6	9.233E-6	8.317E-6	1.264E-5

## Chapter 5

### Summary and Future Work

#### 5.1 Contributions

Inertia estimation methods perform differently at different levels of penetration of renewable energy resources. A power grid with low PV penetration does not have large inertia to prevent system collapse because of retiring traditional synchronous generators. Inertia estimation methods can estimate inertia without a significant error, except for the moment of a disturbance. As PV penetration increases, PV units provide more inertia to the power grid, and it becomes challenging for three inertia estimation methods to estimate inertia because inverter controllers regulates the frequency and other parameters, such as voltage. The Minimum Volume Enclosing Ellipsoid and Back Propagation Neural Network methods cannot estimate inertia at the moment of disturbance because they cannot classify a sudden change in the input features. However, the symbolic aggregate approximation method can classify disturbance data, with an improved overall performance than the other methods.

This thesis introduces a new method for the estimation of system inertia. Unlike the existing complex model-based methods, Symbolic Aggregate Approximation is a measurement-based model that detects the PMU measurement to estimate inertia. Therefore, applying a less complex structure to a power system is one of its advantages. Furthermore, the developed SAX method can reduce the size of the dataset because of the data compression. Compared to SAX, most measurement-based models use a large data pool to classify real-time PMU measurements to estimate inertia. Some methods use dimension reduction to decrease the

size of the data. However, this method loses some information during the process. For SAX, the width of time windows can be flexible to avoid losing too much PMU measurement information while reducing the size of a dataset.

### 5.1.1 Summary

This thesis mainly studies the inertia estimation of renewable energy generators and establishes three measurement-based inertia estimation models. In Chapter 3, a new data-driven inertia estimation method based on symbolic aggregate approximation algorithm was developed to estimate the inertia of a test power grid. The SAX model collects PMU information in the data. Next, the K-nearest Neighbors algorithm is used to estimate the inertia. Two approaches are taken to calculate the inertia: classification and regression. Classification can cluster new PMU data and find relevant data from the dataset to estimate inertia.

The Back Propagation Neural Network method can estimate virtual inertia from the PMU data, and the number of input features relates to the accuracy. Virtual inertia is related to the change in frequency and power deviation and other parameters. Therefore, increasing input features can enhance the accuracy of the method. Meanwhile, the number of layers and neurons also influences performance. The model cannot group input data to correct groups if a structure does not have enough complexity. However, a complicated structure leads to an over-fitting problem. BNN cannot accurately estimate the inertia. As shown in Chapter 4, the BNN method cannot estimate inertia better than SAX, but its performance is better than the Minimum Volume Enclosing Ellipsoid.

The Minimum Volume Enclosing Ellipsoid method can estimate inertia in another power grid without training the model again because it uses a higher-order regression function to estimate inertia for a single unit. However, the method does not perform well compared to the other



methods. This poor performance is due to the fact that a disturbance causes the parameters to oscillate and enhances the challenge of regressing a real-time PMU measurement. Also, a Gradient Descent Machine Learning model is applied to the regression equation to calculate the virtual inertia. Based on the error between the label inertia and the output value, a Gradient Descent Machine Learning model moves the order weight to reduce the error and increase the accuracy.

## 5.2 Future Research Directions

The photovoltaic inverter controllers use the parameters of the grid to control the output parameters. However, those inverters only receive their bus information for regulation. In future work, PVs can receive other generators' status to provide additional output reactive power and enhance power grid stability. Inertia estimation can be another source for PV to regulate abnormal power grid conditions after a disturbance occurs. For example, one synchronous generator and one PV are placed very close. The synchronous generator cannot store enough inertia to compensate for a power imbalance. Then, the PV can produce more reactive power to help the synchronous generator to regulate the power grid.

This thesis has not considered the load variations, However, the load is not constant in the real world. The simulation assumes that all load is constant and observes the impact of photovoltaic systems on system inertia. Similar to renewable generators, the load can also impact power grid stability. Even if the weather does not change, the load variations can create an imbalance in a power grid. In future work, we will investigate the impacts of load variations on the estimated virtual inertia.

## REFERENCES

- [1] W.-S. Im, C. Wang, W. Liu, L. Liu, and J.-M. Kim, “Distributed virtual inertia based control of multiple photovoltaic systems in autonomous microgrid,” *IEEE/CAA Journal of Automatica Sinica*, vol. 4, no. 3, pp. 512–519, 2016.
- [2] K. Y. Yap, C. R. Sarimuthu, and J. M.-Y. Lim, “Virtual inertia-based inverters for mitigating frequency instability in grid-connected renewable energy system: A review,” *Applied Sciences*, vol. 9, no. 24, p. 5300, 2019.
- [3] D. P. Chassin, Z. Huang, M. K. Donnelly, C. Hassler, E. Ramirez, and C. Ray, “Estimation of wecc system inertia using observed frequency transients,” *IEEE Transactions on Power Systems*, vol. 20, no. 2, pp. 1190–1192, 2005.
- [4] B. Tan, J. Zhao, M. Netto, V. Krishnan, V. Terzija, and Y. Zhang, “Power system inertia estimation: Review of methods and the impacts of converter-interfaced generations,” *International Journal of Electrical Power & Energy Systems*, vol. 134, p. 107362, 2022.
- [5] M. Namba, T. Nishiwaki, S. Yokokawa, and K. Ohtsuka, “Identification of parameters for power system stability analysis using kalman filter,” *IEEE Transactions on Power Apparatus and Systems*, no. 7, pp. 3304–3311, 1981.
- [6] H. G. Aghamolki, Z. Miao, L. Fan, W. Jiang, and D. Manjure, “Identification of synchronous generator model with frequency control using unscented kalman filter,” *Electric Power Systems Research*, vol. 126, pp. 45–55, 2015.
- [7] L. Fan and Y. Wehbe, “Extended kalman filtering based real-time dynamic state and parameter estimation using pmu data,” *Electric Power Systems Research*, vol. 103, pp. 168–177, 2013.
- [8] M. González-Cagigal, J. Rosendo-Macías, and A. Gómez-Expósito, “Parameter estimation of fully regulated synchronous generators using unscented kalman filters,” *Electric Power Systems Research*, vol. 168, pp. 210–217, 2019.
- [9] Y. Wehbe, L. Fan, and Z. Miao, “Least squares based estimation of synchronous generator states and parameters with phasor measurement units,” in *2012 North American Power Symposium (NAPS)*. IEEE, 2012, pp. 1–6.

- [10] M. Burth, G. C. Verghese, and M. Velez-Reyes, "Subset selection for improved parameter estimation in on-line identification of a synchronous generator," *IEEE Transactions on Power Systems*, vol. 14, no. 1, pp. 218–225, 1999.
- [11] M. Huang, W. Li, and W. Yan, "Estimating parameters of synchronous generators using square-root unscented kalman filter," *Electric Power Systems Research*, vol. 80, no. 9, pp. 1137–1144, 2010.
- [12] A. Rouhani and A. Abur, "Constrained iterated unscented kalman filter for dynamic state and parameter estimation," *IEEE Transactions on Power Systems*, vol. 33, no. 3, pp. 2404–2414, 2017.
- [13] D. Del Giudice and S. Grillo, "Analysis of the sensitivity of extended kalman filter-based inertia estimation method to the assumed time of disturbance," *Energies*, vol. 12, no. 3, p. 483, 2019.
- [14] G. Valverde, E. Kyriakides, G. T. Heydt, and V. Terzija, "Nonlinear estimation of synchronous machine parameters using operating data," *IEEE Transactions on Energy Conversion*, vol. 26, no. 3, pp. 831–839, 2011.
- [15] E. L. Geraldi, T. C. Fernandes, and R. A. Ramos, "A ukf-based approach to estimate parameters of a three-phase synchronous generator model," *Energy Systems*, vol. 9, no. 3, pp. 573–603, 2018.
- [16] E. L. Geraldi Jr, T. C. Fernandes, A. B. Piardi, A. P. Grilo, and R. A. Ramos, "Parameter estimation of a synchronous generator model under unbalanced operating conditions," *Electric Power Systems Research*, vol. 187, p. 106487, 2020.
- [17] E. P. T. Cari and L. F. C. Alberto, "Parameter estimation of synchronous generators from different types of disturbances," in *2011 IEEE Power and Energy Society General Meeting*. IEEE, 2011, pp. 1–7.
- [18] A. Vahidnia, G. Ledwich, E. Palmer, and A. Ghosh, "Generator coherency and area detection in large power systems," *IET Generation, Transmission & Distribution*, vol. 6, no. 9, pp. 874–883, 2012.
- [19] S. Nabavi and A. Chakraborty, "Structured identification of reduced-order models of power systems in a differential-algebraic form," *IEEE Transactions on Power Systems*, vol. 32, no. 1, pp. 198–207, 2016.
- [20] M. Shiroei, B. Mohammadi-Ivatloo, and M. Parniani, "Low-order dynamic equivalent estimation of power systems using data of phasor measurement units," *International Journal of Electrical Power & Energy Systems*, vol. 74, pp. 134–141, 2016.

- [21] M. Liu, J. Chen, and F. Milano, “On-line inertia estimation for synchronous and non-synchronous devices,” *IEEE Transactions on Power Systems*, vol. 36, no. 3, pp. 2693–2701, 2020.
- [22] P. Makolo, I. Oladeji, R. Zamora, and T.-T. Lie, “Data-driven inertia estimation based on frequency gradient for power systems with high penetration of renewable energy sources,” *Electric Power Systems Research*, vol. 195, p. 107171, 2021.
- [23] F. Zeng, J. Zhang, G. Chen, Z. Wu, S. Huang, and Y. Liang, “Online estimation of power system inertia constant under normal operating conditions,” *IEEE Access*, vol. 8, pp. 101 426–101 436, 2020.
- [24] V. Sagar and S. K. Jain, “System identification-based estimation of power system inertia using pmu data,” in *2020 21st National Power Systems Conference (NPSC)*. IEEE, 2020, pp. 1–6.
- [25] J. Ma, Y. V. Makarov, R. Diao, P. V. Etingov, J. E. Dagle, and E. De Tuglie, “The characteristic ellipsoid methodology and its application in power systems,” *IEEE Transactions on Power Systems*, vol. 27, no. 4, pp. 2206–2214, 2012.
- [26] C. Phurailatpam, Z. H. Rather, B. Bahrani, and S. Doolla, “Estimation of non-synchronous inertia in ac microgrids,” *IEEE Transactions on Sustainable Energy*, vol. 12, no. 4, pp. 1903–1914, 2021.
- [27] J. Zhao, Y. Tang, and V. Terzija, “Robust online estimation of power system center of inertia frequency,” *IEEE Transactions on Power Systems*, vol. 34, no. 1, pp. 821–825, 2018.
- [28] T. Inoue, H. Taniguchi, Y. Ikeguchi, and K. Yoshida, “Estimation of power system inertia constant and capacity of spinning-reserve support generators using measured frequency transients,” *IEEE Transactions on Power Systems*, vol. 12, no. 1, pp. 136–143, 1997.
- [29] C. Phurailatpam, Z. H. Rather, B. Bahrani, and S. Doolla, “Measurement-based estimation of inertia in ac microgrids,” *IEEE Transactions on Sustainable Energy*, vol. 11, no. 3, pp. 1975–1984, 2019.
- [30] S. Guo, S. Norris, and J. Bialek, “Adaptive parameter estimation of power system dynamic model using modal information,” *IEEE Transactions on Power Systems*, vol. 29, no. 6, pp. 2854–2861, 2014.
- [31] P. Makolo, R. Zamora, and T.-T. Lie, “Heuristic inertia estimation technique for power networks with high penetration of res,” in *2020 2nd International Conference on Smart Power & Internet Energy Systems (SPIES)*. IEEE, 2020, pp. 356–361.

- [32] Y. Bian, H. Wyman-Pain, F. Li, R. Bhakar, S. Mishra, and N. P. Padhy, "Demand side contributions for system inertia in the gb power system," *IEEE Transactions on Power Systems*, vol. 33, no. 4, pp. 3521–3530, 2017.
- [33] T. Chen, J. Guo, B. Chaudhuri, and S. Hui, "Virtual inertia from smart loads," *IEEE Transactions on Smart Grid*, vol. 11, no. 5, pp. 4311–4320, 2020.
- [34] D. Yang, B. Wang, G. Cai, Z. Chen, J. Ma, Z. Sun, and L. Wang, "Data-driven estimation of inertia for multiarea interconnected power systems using dynamic mode decomposition," *IEEE Transactions on Industrial Informatics*, vol. 17, no. 4, pp. 2686–2695, 2020.
- [35] K. Tuttelberg, J. Kilter, D. Wilson, and K. Uhlen, "Estimation of power system inertia from ambient wide area measurements," *IEEE Transactions on Power Systems*, vol. 33, no. 6, pp. 7249–7257, 2018.
- [36] B. Wang, D. Yang, G. Cai, J. Ma, Z. Chen, and L. Wang, "Online inertia estimation using electromechanical oscillation modal extracted from synchronized ambient data," *Journal of Modern Power Systems and Clean Energy*, 2020.
- [37] T. Jiang, Y. Mu, H. Jia, N. Lu, H. Yuan, J. Yan, and W. Li, "A novel dominant mode estimation method for analyzing inter-area oscillation in china southern power grid," *IEEE Transactions on Smart Grid*, vol. 7, no. 5, pp. 2549–2560, 2016.
- [38] G. Cai, B. Wang, D. Yang, Z. Sun, and L. Wang, "Inertia estimation based on observed electromechanical oscillation response for power systems," *IEEE Transactions on Power Systems*, vol. 34, no. 6, pp. 4291–4299, 2019.
- [39] T. Jiang, X. Li, H. Yuan, H. Jia, and F. Li, "Estimating electromechanical oscillation modes from synchrophasor measurements in bulk power grids using fssi," *IET Generation, Transmission & Distribution*, vol. 12, no. 10, pp. 2347–2358, 2018.
- [40] P. Wall, F. Gonzalez-Longatt, and V. Terzija, "Estimation of generator inertia available during a disturbance," in *2012 IEEE Power and Energy Society General Meeting*. IEEE, 2012, pp. 1–8.
- [41] P. Wall and V. Terzija, "Simultaneous estimation of the time of disturbance and inertia in power systems," *IEEE Transactions on Power Delivery*, vol. 29, no. 4, pp. 2018–2031, 2014.
- [42] M. Rauniyar, S. Berg, S. Subedi, T. M. Hansen, R. Fournery, R. Tonkoski, and U. Tamrakar, "Evaluation of probing signals for implementing moving horizon inertia estimation in microgrids," in *2020 52nd North American Power Symposium (NAPS)*. IEEE, 2021, pp. 1–6.

- [43] S. Eftekharnajad, V. Vittal, G. T. Heydt, B. Keel, and J. Loehr, “Impact of increased penetration of photovoltaic generation on power systems,” *IEEE transactions on power systems*, vol. 28, no. 2, pp. 893–901, 2012.
- [44] —, “Small signal stability assessment of power systems with increased penetration of photovoltaic generation: A case study,” *IEEE transactions on sustainable energy*, vol. 4, no. 4, pp. 960–967, 2013.
- [45] V. Vittal, J. D. McCalley, P. M. Anderson, and A. Fouad, *Power system control and stability*. John Wiley & Sons, 2019.
- [46] S. B. Kjaer, J. K. Pedersen, and F. Blaabjerg, “Power inverter topologies for photovoltaic modules—a review,” in *Conference Record of the 2002 IEEE Industry Applications Conference. 37th IAS Annual Meeting (Cat. No. 02CH37344)*, vol. 2. IEEE, 2002, pp. 782–788.
- [47] A. Ellis, B. Karlson, and J. Williams, “Utility-scale photovoltaic procedures and interconnection requirements,” *Sandia National Laboratories SAND2012-2090*, 2012.
- [48] A. Ellis, R. Nelson, E. Von Engeln, R. Walling, J. MacDowell, L. Casey, E. Seymour, W. Peter, C. Barker, B. Kirby, and J. R. Williams, “Review of existing reactive power requirements for variable generation,” in *2012 IEEE Power and Energy Society General Meeting*, 2012, pp. 1–7.
- [49] H. Saadat and E. E. Series, *Computational aids in control systems using MATLAB*. McGraw-Hill, 1993.
- [50] A. Fernández-Guillamón, A. Viguera-Rodríguez, and Á. Molina-García, “Analysis of power system inertia estimation in high wind power plant integration scenarios,” *IET Renewable Power Generation*, vol. 13, no. 15, pp. 2807–2816, 2019.
- [51] R. Ma, “Enhancing grid reliability with phasor measurement units,” Ph.D. dissertation, Syracuse University, 2022.
- [52] H. R. Chamorro, A. D. Orjuela-Cañón, D. Ganger, M. Persson, F. Gonzalez-Longatt, V. K. Sood, and W. Martinez, “Nadir frequency estimation in low-inertia power systems,” in *2020 IEEE 29th International Symposium on Industrial Electronics (ISIE)*. IEEE, 2020, pp. 918–922.
- [53] G. S. E. Solutions, “Power factor and grid-connected photovoltaics,” *GSES Technical Papers, ed*, 2016.
- [54] L. Jin, X. Gong, Q. Sun, and M. Sha, “Reactive power control of grid-connected photovoltaic power generation,” in *Journal of Physics: Conference Series*, vol. 1754, no. 1. IOP Publishing, 2021, p. 012001.

- [55] I. C. Report, “Computer representation of excitation systems,” *IEEE Transactions on Power Apparatus and Systems*, no. 6, pp. 1460–1464, 1968.
- [56] —, “Excitation system models for power system stability studies,” *IEEE Transactions on Power Apparatus and Systems*, vol. PAS-100, no. 2, pp. 494–509, 1981.
- [57] H. Cui, F. Li, and K. Tomsovic, “Hybrid symbolic-numeric framework for power system modeling and analysis,” *IEEE Transactions on Power Systems*, vol. 36, no. 2, pp. 1373–1384, 2020.
- [58] T. Xu, A. B. Birchfield, K. S. Shetye, and T. J. Overbye, “Creation of synthetic electric grid models for transient stability studies,” in *The 10th Bulk Power Systems Dynamics and Control Symposium (IREP 2017)*, 2017, pp. 1–6.
- [59] P. Pourbeik, J. J. Sanchez-Gasca, J. Senthil, J. D. Weber, P. S. Zadehkhosht, Y. Kazachkov, S. Tacke, J. Wen, and A. Ellis, “Generic dynamic models for modeling wind power plants and other renewable technologies in large-scale power system studies,” *IEEE Transactions on Energy Conversion*, vol. 32, no. 3, pp. 1108–1116, 2016.
- [60] W. R. E. M. T. Force, “Wecc pv power plant dynamic modeling guide,” *Western Electricity Coordinating Council*, 2014.
- [61] P. WECC, “Power plant dynamic modeling guide,” *WECC Renewable Energy Modeling Task Force*, 2014.
- [62] A. Ellis, Y. Kazachkov, E. Muljadi, P. Pourbeik, and J. Sanchez-Gasca, “Description and technical specifications for generic wtg models—a status report,” in *2011 IEEE/PES Power Systems Conference and Exposition*. IEEE, 2011, pp. 1–8.
- [63] E. R. Paidi, H. Marzoghi, J. Yu, and V. Terzija, “Development and validation of artificial neural network-based tools for forecasting of power system inertia with wind farms penetration,” *IEEE Systems Journal*, vol. 14, no. 4, pp. 4978–4989, 2020.

## **VITA**

Name of Author: Che Kai Chang

Place of Birth: Taiwan

Major: Electrical Engineering

## **Education**

M.S., Dec 2022, Syracuse University, United State (expected)

B.S., Jun 2018, Chung Yuan Christian University, Taiwan